

**OPTIMAL ORIENTATION AND TILTING
ANGLE OF PV PANELS CONSIDERING
SHADING AND TEMPERATUTE EFFECTS**

CHONG BOON YOONG

UNIVERSITI TUNKU ABDUL RAHMAN

**OPTIMAL ORIENTATION AND TILTING ANGLE OF PV PANELS
CONSIDERING SHADING AND TEMPERATURE EFFECTS**

CHONG BOON YOONG


**A project report submitted in partial fulfilment of the
requirements for the award of Bachelor of Electrical and Electronic
Engineering with Honours**

**Lee Kong Chian Faculty of Engineering and Science
Universiti Tunku Abdul Rahman**

May 2023

DECLARATION

I hereby declare that this project report is based on my original work except for citations and quotations which have been duly acknowledged. I also declare that it has not been previously and concurrently submitted for any other degree or award at UTAR or other institutions.

Signature : 

Name : CHONG BOON YOONG

ID No. : 18UEB03849

Date : 8-5-2023

APPROVAL FOR SUBMISSION

I certify that this project report entitled "**OPTIMAL ORIENTATION AND TILTING ANGLE OF PV PANELS CONSIDERING SHADING AND TEMPERATURE EFFECTS**" was prepared by **CHONG BOON YOONG** has met the required standard for submission in partial fulfilment of the requirements for the award of Bachelor of Electrical and Electronic Engineering with Honours at Universiti Tunku Abdul Rahman.

Approved by,

Signature :  _____

Supervisor : Ir. Dr. Lim Boon Han

Date : 8-5-2023

Signature : _____

Co-Supervisor : _____

Date : _____

The copyright of this report belongs to the author under the terms of the copyright Act 1987 as qualified by Intellectual Property Policy of Universiti Tunku Abdul Rahman. Due acknowledgement shall always be made of the use of any material contained in, or derived from, this report.

© 2023, CHONG BOON YOONG. All right reserved.

ACKNOWLEDGEMENTS

I would like to thank everyone who had contributed to the successful completion of this project. I would like to express my gratitude to my research supervisor, Ir. Dr. Lim Boon Han for his invaluable advice, guidance, and patience throughout the research development.

In addition, I would also like to express my gratitude to my loving parents and friends who had helped and given me encouragement and support throughout this entire journey. Without them, I would not have been able to complete this project successfully.

I would like to extend my appreciation to the University staff and faculty members who provided me with access to the resources necessary for this study. Their assistance and support were vital in enabling me to complete this study.

Thank you all once again for your invaluable support and contributions to this project. I am truly grateful for everything that you have done for me.

ABSTRACT

The optimal orientation and titling angle of the photovoltaic (PV) panels are crucial for maximizing their energy output and ensuring a great return on the investment for solar power systems. This report investigates the crucial relationship between optimal orientation, tilting angle, shading, and module temperature in the context of PV output performance. The main objective is to determine PV panels' optimal orientation and tilting angle to maximize energy generation while considering shading and temperature effects. The investigation location is at Universiti Tunku Abdul Rahman (UTAR), Bandar Sungai Long. Three transposition sky models, converting global horizontal irradiance to global tilted irradiance, are utilized and compared to estimate global tilted irradiance, while a simple 2-D trigonometric approach is proposed for calculating the shading factor. The conventional Ross coefficient model is used to predict the module operating temperature and its impact on PV performance. The results show that the optimal tilting angle of PV array depends on the DL (distance between two rows of PV array to the panel length) ratio and panel configuration, considering shading effects with bypass diodes. The optimal surface azimuth angle is slightly South of due East (104° - 122°). Although the temperature effect does not significantly impact the optimal PV positioning, it does decrease the Reduced Equivalent Solar Irradiation due to Temperature Effect (RESIT) yielded in all directions. The suggested DL ratio is around 1.3 with the landscape 4-stacked configuration to minimize shading and loss. This study hopes to provide the solar industry with a guideline for installing PV panels at optimal orientation and tilting angles while considering shading and temperature effects to yield maximum PV output in Malaysia.

TABLE OF CONTENTS

DECLARATION		i
APPROVAL FOR SUBMISSION		ii
ACKNOWLEDGEMENTS		iv
ABSTRACT		v
TABLE OF CONTENTS		vi
LIST OF TABLES		ix
LIST OF FIGURES		x
LIST OF SYMBOLS / ABBREVIATIONS		xii
LIST OF APPENDICES		xv
CHAPTER		
1	INTRODUCTION	16
1.1	General Introduction	16
1.2	Importance of the Study	17
1.3	Problem Statement	18
1.4	Aim and Objectives	19
1.5	Scope and Limitation of the Study	19
1.6	Contribution of the Study	20
1.7	Outline of the Report	20
2	LITERATURE REVIEW	21
2.1	Introduction	21
2.2	Literature Review	21
2.2.1	Solar Position	21
2.2.2	Solar Irradiance	22
2.2.3	Transposition Model	23
2.2.4	Research on Optimal Tilt Angle and Orientation of PV Panels	24
2.2.5	Research on Shading Factor Calculation	28

	2.2.6 Research on Temperature Effect on the PV Performance	34
	2.3 Summary	41
3	METHODOLOGY AND WORK PLAN	46
	3.1 Introduction	46
	3.2 Flowchart of Work	47
	3.3 Irradiance Data	50
	3.3.1 Satellite-derived Data	50
	3.3.2 Ground-based Solar Irradiance Measurement	51
	3.4 Modelling of Solar Irradiance on Tilted Surfaces	52
	3.4.1 Modelling of Tilted Direct Irradiance	52
	3.4.2 Modelling of Tilted Diffuse Irradiance	56
	3.5 Modelling of Reduced Equivalent Solar Irradiance (RESI)	59
	3.5.1 Reduced Equivalent Solar Irradiance due to Shading–Bypass Diode (RESIS)	59
	3.5.2 Reduced Equivalent Solar Irradiance due to Temperature (RESIT)	60
	3.6 Determining the Optimal Tilt Angle and Orientation	61
	3.7 Statistical Evaluation	62
	3.8 Work Plan	63
	3.9 Summary	64
4	RESULTS AND DISCUSSION	65
	4.1 Introduction	65
	4.2 Comparison between the Empirical Models	66
	4.3 Relationship between Different DL Ratios and Shading Effect	68
	4.4 Comparison between Different PV Orientation Configurations	70
	4.5 Temperature Effect	76
	4.6 Temperature Effect and Shading Effect with Bypass Diode	78

4.7	Study on the Input Solar Irradiance Data and Optimal PV Positioning	79
4.8	Summary	88
5	CONCLUSIONS AND RECOMMENDATIONS	89
5.1	Conclusions	89
5.2	Recommendations for future work	90
	REFERENCES	92
	APPENDICES	96

LIST OF TABLES

Table 2.1:	Monthly and Seasonal Optimal Tilt Angles for the Five Cities	26
Table 2.2:	Range of Annual PV Performance Loss due to Temperature Effect for the Different Mounting Systems in 18 PV Plants	36
Table 2.3:	List of Temperature Coefficient Range for Crystalline Silicon PV Module	37
Table 2.4:	Overall and Time-specific Ross Coefficients for Different Mounting Types	38
Table 2.5:	Ross Coefficients for Different Mounting Types	39
Table 2.6:	Details of the Methods/Models Used to Determine the Optimal Tilt Angle and Orientation	41
Table 2.7:	Details of the Methods/Models Used to Determine the Shading Factor and Row Spacing	43
Table 2.8:	Summary of the Temperature Effect on the PV Performance and the Temperature Model	45
Table 4.1:	Optimal Tilting Angle and Orientation, and Maximum GTI Yielded for Different Sky Models at DL Ratio of 1.2.	81
Table 4.2:	Summary Table for Optimal Tilting Angle and Orientation, and Maximum RESIS Yielded for Different Types of Horizontal Solar Irradiance Data using Perez Model with Landscape 2-stacked Configuration and DL Ratio of 1.4.	82

LIST OF FIGURES

Figure 2.1:	Shading Factor Table Used in PVsyst	29
Figure 2.2:	Current Flow in PV Module with One Shaded Cell	33
Figure 2.3:	Scatter Plots between the Measured and Estimated Module Temperature	40
Figure 3.1:	Work Flowchart	49
Figure 3.2:	Irradiance Measurement on Horizontal Surface.	51
Figure 3.3:	3D Representation of the Inter-row Shading	54
Figure 3.4:	Rectangular Plane Including the Shadow Projection	55
Figure 3.5:	Top View of the 3D Representation of Inter-row Shading	55
Figure 3.6:	Coefficients of Perez Model	58
Figure 3.7:	Effect of Partial Shading for Different Panel Configurations	60
Figure 3.8:	Gantt Chart for the Project	63
Figure 4.1:	Analysis and Discussion Scope	65
Figure 4.2:	Annual GTI for Different Sky Models	66
Figure 4.3:	Percentage Difference between Sky Models	66
Figure 4.4:	Annual Diffuse Irradiation on the Titled Surface for Different Sky Models	67
Figure 4.5:	Annual GTI for Different DL Ratios.	68
Figure 4.6:	Effect of DL Ratio on the Inter-row Shading Loss	69
Figure 4.7:	Effect of DL Ratio on the Maximum Annual GTI, PV Optimal Tilt and Surface Azimuth Angles	70
Figure 4.8:	RESIS Polar Contour Plots for Different Stack Numbers of Landscape-oriented Panel	71
Figure 4.9:	Graphs of Shading Loss against Partial Shading for Landscape-oriented PV	72

Figure 4.10:	RESIS Polar Contour Plots for Different Stack Number of Portrait-oriented Panel	72
Figure 4.11:	Graphs of Shading Loss against Partial Shading for Portrait-oriented PV	72
Figure 4.12:	Shading Loss due to Bypass Diode for Different Panel Configuration. Note: The Abbreviation Meaning: PT: Portrait 1-stacked; PT 2-S: Portrait 2-stacked; LS: Landscape 1-stacked; LS 2-S: Landscape 2-stacked; LS 3-S: Landscape 3-stacked; and LS 4-S: Landscape 4-stacked.	73
Figure 4.13:	Shading Loss due to Bypass Diode for Different Panel Configurations and DL Ratios	74
Figure 4.14:	(a) Optimal Tilt Angle and (b) Surface Azimuth Angle for Different Panel Configurations and DL Ratio	75
Figure 4.15:	Comparison between RESIT and GTI Contour Plots	76
Figure 4.16:	Optimal Tilt Angle and Surface Azimuth Angle Considering Temperature Effect	77
Figure 4.17:	Effect of DL ratio on the drop in RESI due to temperature effect.	77
Figure 4.18:	RESI Drop due to Temperature and Shading Effects with Bypass Diode for Different Panel Configurations and DL Ratios.	78
Figure 4.19:	(a) Optimal Tilt Angle and (b) Surface Azimuth Angle for Different Panel Configurations and DL Ratio Considering Temperature and Shading Effects.	79
Figure 4.20:	Optimal Tilt Angle, Surface Azimuth and Maximum Solar Irradiation (or RESIS) Estimated using Solargis TMY and 20-year Time Series Data.	85
Figure 4.21:	Optimal Tilt Angle, Surface Azimuth and Maximum Solar Irradiation (or RESIS) Estimated Based on Solargis Time Series Data and Ground-based Measurement Data Using Hay and Davies Model for Year 2020	87

LIST OF SYMBOLS / ABBREVIATIONS

$\cos \theta$	cosine efficiency
h_s	solar height, m
A_i	anisotropic index
\vec{I}	solar radiation vector
I_0	extra-terrestrials radiation, W/m^2
I_b	direct irradiance on tilted surface, W/m^2
I_d	tilted diffuse irradiance, W/m^2
I_r	in-plane solar irradiance, W/m^2
\vec{N}	normal vector of the PV module surface
P_{max1}	PV maximum output power before considering temperature effect, W
P_{max2}	PV maximum output power after considering temperature effect, W
$X_{n,1}$	entries of data set 1 or reference set
$X_{n,2}$	entries of data set 2
f_s	shading factor
f_{temp}	temperature factor
k_{Ross}	Ross coefficient, $^{\circ}C/(W/m^2)$
t_a	ambient temperature, $^{\circ}C$
t_m	PV module operating temperature, $^{\circ}C$
α_t	temperature coefficient of current, $\%/^{\circ}C$
β_t	temperature coefficient of voltage, $\%/^{\circ}C$
θ_p	PV azimuth angle, $^{\circ}$
θ_s	solar azimuth angle, $^{\circ}$
θ_z	solar zenith angle, $^{\circ}$
Δh	height difference between two adjacent arrays, m
2-D	two-dimensional
3-D	three-dimensional
ASHRAE IWEC 1.1	American Society of Heating, Refrigerating and Air-Conditioning Engineer International Weather for Energy Calculations Version 1.1

BIPV	Building Integrated Photovoltaic
DL Ratio	pitch-distance-to-PV-length ratio
EPLISSI	Liogu Ku Silou-Silou
GHI	global horizontal irradiance, W/m^2
GTA	Greater Toronto Area
GTI	global tilted irradiance, W/m^2
h	module height, m
HAPD	highest absolute percentage difference, %
HDKR	Hay, Davies, Klucher, and Reindl
LS 2-S	landscape 2-stacked
LS 3-S	landscape 3-stacked
LS 4-S	landscape 4-stacked
LS	landscape 1-stacked
LSS	large-scale solar program
MAD	mean absolute difference
MAE	mean absolute error
MAPD	mean absolute percentage difference, %
METPV-11	MEteorological Test Data for PhotoVoltaic Version 11 system
MUT	module under test
NASA SSE	National Aeronautics and Space Administration, Surface Meteorology and Solar Energy program
NEM	net energy metering
NiMet	Nigerian Meteorological Agency
NOCT	normal operating cell temperature
NREL	National Renewable Energy Laboratory
NRMSE	normalized root mean square error
PT 2-S	portrait 2-stacked
PT	portrait 1-stacked
PV	photovoltaic
RESI	reduced equivalent solar irradiation, kWh/m^2
RESIS	reduced equivalent solar irradiance due to shading- bypass diode, kWh/m^2

RESIT	reduced equivalent solar irradiance due to temperature, kWh/m ²
RMSD	root mean square difference
RMSE	root mean square error
SAM	System Advisor Model
SERI	Solar Energy Research Institute
SWERA	Solar and Wind Energy Resource Assessment Program
TIF	feed-in tariff
TMY	Typical Meteorological Year
UKM	Universiti Kebangsaan Malaysia
UTAR	University of Tunku Abdul Rahman
VBA	Visual Basic Application
WRMC	World Radiation Monitoring Centre
<i>AOI</i>	angle of incidence, °
<i>DHI</i>	diffuse horizontal irradiance, W/m ²
<i>DNI</i>	direct normal irradiance on horizontal surface, W/m ²
<i>F1</i>	circumsolar brightness coefficient
<i>F2</i>	horizon brightness coefficient
<i>d</i>	row spacing, m
<i>f</i>	multiplier factor
<i>l</i>	module length, m
<i>α</i>	solar altitude angle, °
<i>β</i>	tilt angle, °
<i>γ</i>	temperature coefficient of maximum power, %/°C
<i>δ</i>	declination angle, °
<i>ω</i>	hour angle, °
<i>φ</i>	site latitude, °

LIST OF APPENDICES

Appendix A: Flowchart for Processing 20-year Solargis Time Series Data	96
---------------------------------------------------------------------------	----

CHAPTER 1

INTRODUCTION

1.1 General Introduction

Solar energy is a sustainable and limitless energy source that can replace fossil fuel power generation to reduce greenhouse gas emissions and mitigate global warming. It can be transformed into usable electrical energy by using photovoltaic (PV) panels. In the effort to attain a carbon-neutral environment, the Malaysian government established various schemes and initiatives, such as large-scale solar program (LSS), feed-in tariff (FIT), net energy metering (NEM), etc., to promote awareness of utilising solar energy (seda.gov.my, 2022)

The performance of the PV is greatly affected by many external factors, namely the ambient temperature, tilting angle, orientation, shading, glass reflection, and electrical conversion efficiency. Among all those factors, the amount of solar irradiance reaching the PV module surface depends majorly on the tilt angle and orientation chosen for installation. Hence, it is necessary to determine the optimal positioning of the PV to harness the maximum solar radiation possible. A good rule of thumb and the conventional approach of tilting a PV module is based on the location's latitude, facing towards the equator. However, it is proven inaccurate due to the sun's seasonal trajectory (Yakup and Malik, 2001).

A large-scale solar farm consists of multiple rows of PV arrays separated by distance spacing, also known as inter-row spacing. The shadow projection of a collector may be cast on the adjacent PV rows, depending on the pitch distance, tilt angle, module length and height, and geographical latitude (Appelbaum and Bany, 1979). This shading effect is undesirable as the direct sunlight will be obstructed, reducing the amount of solar insolation received by the PV module and decreasing the module's efficiency.

Furthermore, the PV module operating temperature can significantly influence the PV performance, as a higher temperature will deteriorate the output power produced. According to a study conducted by Soliman et al. (2020), the PV efficiency could reduce by about 10 % due to the rise in module operating temperature. A PV module's operating temperature depends on

various factors such as the type of cell technologies, in-plane solar irradiance, ambient temperature, and other related parameters.

In the context of PV output performance, a crucial relationship exists between optimal orientation and tilting angle, shading, and module temperature. The PV panels' optimal orientation and tilting angle are primarily geometrical issues significantly affecting electricity generation. Conversely, the interrow shading can lead to a considerable mismatch loss in the PV panels. The amount of shading is always inversely proportional to the interrow spacing and land usage. Therefore, higher tilting angles necessitate larger interrow spacings to minimise the shading effect.

Moreover, the PV panels are interconnected with bypass diodes that exhibit non-linear behaviour with respect to the solar irradiance received. This non-linearity can cause significant variations in the electrical output of the PV panels. As a result, it is imperative to optimise the PV installation angle to reduce the impact of the shading on the bypass diodes' non-linearity.

Lastly, the module operating temperature cannot be disregarded. When the PV orientation and tilting angle are not optimal, the loss due to temperature is also reduced. Although all these relationships may not be proportional, this project aims to investigate the optimal orientation and tilting angle of PV panels considering the shading and temperature effects to maximise the PV energy generation.

1.2 Importance of the Study

One of the cost-effective ways to install PV systems is to have them fixed at the optimal position, especially in the tropics. Hence, it is critical to determine the best positioning of the PV systems to yield maximum solar irradiation. Implementing sun tracking technology, which can follow the sun's trajectory for any particular season throughout the year, can increase the energy output yielded. Nevertheless, the gain in energy output depends on the amount of direct irradiance. In the tropics, this gain is reduced due to the high diffuse irradiance. As such, the potential benefits of sun-tracking systems in tropical regions are less pronounced because of the same additional cost with less gain.

In most of the PV research, the optimal tilting angle and orientation are often determined based on the in-plane solar irradiance. However, this approach

is overly idealistic as it does not consider practical factors such as shading and temperature effect. Accounting for these factors will provide results closer to the theoretical predictions. In practice, the design of the PV system should also consider the ohmic loss and inverter efficiency, which can be controlled, but the temperature and shading effect require necessary simulations to determine the optimal solutions. Therefore, it is essential to simulate and evaluate the PV system under realistic conditions by considering temperature and shading effects to achieve optimal performance.

With the result found, this study hopes to give the industry a guideline to install at optimal orientation and tilting angles to yield the maximum output of PV by considering the losses due to shading and temperature.

1.3 Problem Statement

In determining the optimal tilt angle and orientation, numerous models were presented in the past to estimate the global tilted irradiance from the horizontal solar irradiance.

- While geometric relations are used to calculate direct components of radiation on an inclined plane, different models have been developed to tackle the complexity of converting diffuse components. Based on the assumption of the isotropic distribution of the diffuse radiation in the sky dome, the earliest transposition model is widely used in most research due to its simplicity. Nonetheless, this assumption is not entirely accurate (Loutzenhiser et al., 2007).
- In Malaysia, despite many studies conducted to find the optimal tilt angles in various locations (Fadaeenejad et al., 2015; Jacobson and Jadhav, 2018; Matius et al., 2021), the default South facing is assumed to be the optimal surface orientation.
- Much research has been conducted to propose mathematical models for computing the shading factors that reduce the PV's efficiency; however, fewer studies integrate both the shadow effect and the optimal positioning of the PV system.

- There is insufficient research on the combined analysis of shading loss caused by bypass diode and the temperature effect of the PV modules.

1.4 Aim and Objectives

This project aims to find the optimal tilt angle and orientation of the PV system in considering the shading and temperature effects. The detailed objectives of this project are listed as follows:

- To determine the annual solar irradiation on a tilted surface based on the isotropic and anisotropic models for all possible surface azimuth and tilt angles.
- To investigate the shading and temperature effects on the optimal orientation and tilting angles.
- To compare between the optimal orientation and tilting angles of a PV system computed using the empirical and measured data.

1.5 Scope and Limitation of the Study

This project focuses on determining the optimal tilt angle and orientation of the crystalline silicon PV module for a large-scale solar farm by considering the shadow and temperature effects. The installation of the PV module is assumed to be on flat terrain only. Three transposition models will be utilised to estimate the global tilted irradiance from the horizontal solar irradiance. In addition, a simple 2-D trigonometric approach for calculating the shading factor is proposed. The typical Ross coefficient model will be utilised to estimate the module operating temperature to study its impact on PV performance.

The empirical and measured horizontal solar irradiance data will be used, and the results will be compared and analysed. Nonetheless, this project has several limitations, such as a lack of data availability from a PV site to be used to validate the estimated results and the resolution of the data used.

1.6 Contribution of the Study

This study has investigated the shading loss for different panel configurations with the effect of bypass diodes and analysed the electricity generation loss due to the temperature effect by using a Ross coefficient model to predict the module operating temperature. The study results can provide the solar industry with a design guideline to obtain a PV system's optimal orientation and tilt angle that can yield maximum output by considering losses due to shading and temperature.

Through this research, it is hoped that the PV industry will benefit from the findings, leading to more efficient and cost-effective PV systems in the future.

1.7 Outline of the Report

In this report, five main chapters present the study on the optimal orientation and the tilting angle of PV panels considering the shading and temperature effects.

Chapter 1 introduces solar energy and PV panels, highlighting the factors affecting PV output efficiency. It also emphasises the importance of studying these factors and lists the scope and limitations of the study.

Chapter 2 presents a literature review, which begins with describing some terminologies related to the study. The chapter reviews the existing research on the optimal tilt angle and orientation of the PV panels, shading factor calculation and temperature effect.

Chapter 3 describes the work plan and methodology for the study, including transposition modelling, shading factor modelling, and temperature factor modelling.

Chapter 4 presents the results and discussion of the study, analysing the effects of the shading and temperature on the PV performance. This chapter also compares the optimal orientation and tilting angles of a PV system computed using empirical and measured data.

Finally, Chapter 5 provides a conclusion summarising the study's findings and suggests areas for future research.

CHAPTER 2

LITERATURE REVIEW

2.1 Introduction

The performance of a PV system is correlated to the amount of solar radiation that reaches the PV modules; hence the tilt angle and orientation for fixed array installation are crucial elements. Multiple research projects have been conducted to identify the optimal tilt and orientation at various locations. In addition, the shading and temperature effects are also significant issues that will reduce the output power generation of the PV. Inter-row shading is the typical type of partial shading on PV that most of the studies focused on and formulated out the respective models. Furthermore, the temperature effect on the PV performance will be reviewed.

In this chapter, several important terminologies will be described to provide a brief understanding of sun position, solar radiation, and transposition models.

2.2 Literature Review

2.2.1 Solar Position

The solar intensity varies greatly depending on the sun's position relative to the observer's viewpoint on the surface of the earth. When the solar altitude angle is small, the incident rays travel through more atmosphere compared to that when the sun is straight above. Air mass can be used to quantify the solar irradiance path as it is defined as the ratio of the actual radiation path to the shortest path.

The solar altitude angle, α_s , or the sun elevation angle is denoted as the angle between the horizontal plane and the central sunray, which can be calculated using Equation (1.1). The solar azimuth angle, θ_s , is defined as the angle measured on the horizontal plane whereby the north can be 0 or 360 °, 90 ° east, 180 ° south, and 270 ° west. Equation (1.2) and (1.3) are used to determine the solar azimuth angle.

$$\alpha_s = \sin^{-1}(\sin \delta \sin \phi + \cos \omega \cos \delta \cos \phi) \quad (1.1)$$

If $(\sin \delta \cos \phi - \cos \omega \cos \delta \sin \phi) / \cos \alpha_s > 0$:

$$\theta_s = \sin^{-1} \left(-\frac{\sin \omega \cos \delta}{\cos \alpha_s} \right) \quad (1.2)$$

If $(\sin \delta \cos \phi - \cos \omega \cos \delta \sin \phi) / \cos \alpha_s < 0$:

$$\theta_s = 180^\circ - \sin^{-1} \left(-\frac{\sin \omega \cos \delta}{\cos \alpha_s} \right) \quad (1.3)$$

where

α = solar altitude angle, $^\circ$

θ_s = solar azimuth angle, $^\circ$

ϕ = site latitude, $^\circ$

δ = declination angle, $^\circ$

ω = hour angle, $^\circ$

2.2.2 Solar Irradiance

Solar irradiance is the amount of energy emitted by the sun as electromagnetic radiation per unit area of the surface of the earth (in the unit of W/m^2). It can be used to simulate the maximum power generation of a PV system at any particular time in any given location. There are generally two main types of solar radiation: direct and diffuse irradiance. The direct irradiance, also known as the beam component, originates directly from the disc of the sun. It represents most solar energy, typically up to 80 or 90 %, reaching the earth's surface during a clear day (Stein et al., 2012). The direct irradiance flux reaching a surface that is perpendicular to the solar direction is measured as the direct normal irradiance (DNI). Besides, the diffuse horizontal irradiance (DHI) refers to the portion of solar radiation that reaches the earth after being scattered by the atmosphere in all directions. It can be seen coming from all directions across the whole sky. Hence, this explains the skylight and presence of light on a cloudy day. On a cloudy day or in the shade, most of the solar power generation comes from

diffuse irradiance. In addition, the ground reflections, which vary with surface albedo, are also one of the diffuse components.

The global horizontal irradiance (GHI) represents the sum of the solar radiation on a horizontal surface, while the global tilted irradiance (GTI), as its name implies, refers to the total solar radiation on a tilted surface. The GHI can be computed by summing the DHI on a horizontal surface with the DNI which is multiplied by the cosine of the angle of incidence (AOI). The calculation of the GTI, on the other hand, will involve the transposition model.

2.2.3 Transposition Model

Predicting the GTI for different PV tilt angles and orientations is important to estimate the energy output of a PV system and ensure that the system design can achieve long-term average performance. The transposition models, also called yield estimation models, are widely utilised in the PV industry to predict the GTI on slanted PV modules based on GHI and DHI. The models will transpose the three main irradiance components: DNI, DHI, and albedo, on a horizontal surface to the irradiance on a slanted surface.

In general, the DNI can be calculated by the geometric relationship between the horizontal and inclined planes. The albedo can be estimated by using the isotropic model. Nevertheless, the diffuse component estimation is complicated as it involves complex angular dependencies such as the solar altitude angle and the presence of clouds. In the early models, the conversion of DHI to the slanted surface was made with the assumption of an isotropic distribution of the total sky diffuse irradiance throughout the sky-dome (e.g., Liu and Jordan, 1961). This presumption, however, is oversimplified and at odds with reality. Adapting to more recent transposition models, the diffuse component is dispersed anisotropically. There are some which contemplate both the circumsolar and isotropic components (e.g., Hay and Davies, 1980), whereas others additionally account for horizon-brightening (e.g., Perez et al., 1990).

2.2.4 Research on Optimal Tilt Angle and Orientation of PV Panels

As the receiving maximum solar irradiance by the PV modules is significantly dependent on the tilt angle and orientation of the modules, many researchers from various countries proposed different approaches or models to select the best tilt angle and orientation for the PV system. Mamun et al. (2017) implemented a numerical method for the optimisation angle of the PV panel, using System Advisor Model (SAM) simulation software, to generate the characteristic curves of the annual energy against the surface tilt angle. From the curves, the optimal tilt angle for eight cities in Bangladesh was determined by finding out the tilt angle which could give maximum solar energy. However, this study neglected diffuse and ground-reflected components.

Abdullahi et al. (2020) considered both the direct and diffuse components in the study of determining the optimal PV tilt angle in Kano, Nigeria. They found that the optimal tilt angle of the fixed PV panel was equal to the site's latitude using the Liu and Jorden model based on the Nigerian Meteorological Agency (NiMet) solar irradiance data on the horizontal surface. Nevertheless, the isotropic models, such as Liu and Jordan, as their names imply that the diffuse radiation is assumed to be isotropic only, whereby the horizon brightening and circumsolar are taken as zero. This is not realistic in practical, but the modelling equation is much simpler and more direct. On the other hand, the anisotropic models, which consist of both isotropic and circumsolar components (maybe including the horizon brightening), will be more accurate in reflecting the actual solar radiation distribution compared to the former.

Hailu and Fung (2019) conducted a study on obtaining the optimal tilt angle and orientation of a PV module in the Greater Toronto Area (GTA), Canada by using four isotropic models (Liu and Jorden, Badescu, Tian, and Koronakis) and four anisotropic models (Reindl, Skartveit and Olseth, Steven, M.H. Unsworth, and Hay and Davies). All the solar irradiance data on a horizontal surface for GTA, obtained from the Meteonorm Global Meteorological Database Version 7, were used to compute the GTI for different tilt angles for each month. The annual optimal tilt angle for south-oriented surfaces using the isotropic models was found in the range of 37 ° to 44 °, while that of using the anisotropic models was in the range of 46 ° to 46.5 °. The panel orientation could be adjusted within the range of $\pm 15^\circ$ due south, with less than

1 % reduction in maximum solar irradiance received. This study clearly shows that the optimal tilt angle will be affected by different sky models being used, as each reflects the different distribution of solar radiation.

There are several studies related to the optimisation of the tilt angle of the PV modules in Malaysia. Khatib et al. (2015) presented the optimisation of the tilt angle for five cities in Malaysia, namely Alor Setar, Ipoh, Kuala Lumpur, Johor Bharu, and Kuching. Liu and Jordan model was deployed to determine solar irradiance on tilted surfaces considering monthly and seasonal tilting. Thirty-year historical data from Solar Energy Research Institute (SERI), Universiti Kebangsaan Malaysia (UKM) were used to provide the GHI and DHI for optimal tilt angle computation. Table 2.1 shows the results of the monthly and seasonal optimal tilt angles for the five cities. These results may be feasible for industry only if the panel is oriented towards the south. The optimal orientation is not investigated in the study.

Fadaeenejad et al. (2015) also applied the Liu and Jordan model to identify the monthly and fixed optimal tilt angle for three rural sites in Selangor, Sabah, and Sarawak. They used the solar irradiance on the horizontal surface from the National Aeronautics and Space Administration, Surface Meteorology and Solar Energy program (NASA SSE) PV and considered four different tilt angles (0° - 15°) only, facing towards the south. The fixed optimal slopes of PV for villages in Selangor, Sabah, and Sarawak were 0° , 5° , and 0° , respectively. Nevertheless, the authors utilised the step interval of 5° for tilting in the study, which is quite large, and the results may not be optimal. Apart from that, Matius et al. (2021) conducted a study using four types of isotropic models, Liu and Jordan, Koronakis, Badescu, and Tian models to access the optimal tilt angle in Liogu Ku Silou-Silou (EPLISSI), Sabah. The result suggested that the suitable annual tilt angle was 8.05° with the south-facing orientation.

Table 2.1: Monthly and Seasonal Optimal Tilt Angles for the Five Cities
(Khatib et al., 2015)

Cities	Monthly Optimal Tilt Angle	Seasonal Optimal Tilt Angle	
		Wet (Oct to Mar)	Dry (Apr to Sept)
Alor Setar	0 ° - 32 °	23 °	0 °
Ipoh	0 ° - 28 °	19 °	0 °
Kuala Lumpur	0 ° - 29 °	19 °	0 °
Johor Bharu	0 ° - 24 °	17 °	0 °
Kuching	0 ° - 22 °	15 °	0 °

Besides, Jacobson and Jadhav (2018) provided estimates of the optimal PV tilt angle for all countries worldwide by deriving from the PVWatts program in National Renewable Energy Laboratory (NREL). The PVWatts would utilise the weather and solar irradiance data from the American Society of Heating, Refrigerating and Air-Conditioning Engineer International Weather for Energy Calculations Version 1.1 (ASHRAE IWEC 1.1), and Solar and Wind Energy Resource Assessment Program (SWERA) to estimate the annually averaged solar output for most of the counties by assuming a certain tilt angle value. The optimal tilt angle for each location could be then determined by computing the PV output, which gave the maximum values. However, the orientation of the PV was assumed to be facing the true south (towards the equator). From their finding, the optimal PV tilt angle for Kuala Lumpur was 1 °. Another research done by Elhassan et al. (2011) found that the annual optimal PV tilt angle for Kuala Lumpur was about 15 °, facing the south. Based on the one-year recorded weather data and the average output power of the PV panels, they concluded that the optimal tilt angles and orientations were 15 °, 30 °, and 90 °E, 180 °S for different times of the day.

Despite the same location, e.g., Kuala Lumpur, the optimal tilt angle found was different. This is because different considerations were made in the studies; for example, Elhassan et al. (2011) considered only three tilt angles of 15 °, 20 °, and 30 ° in their studies, while Jacobson and Jadhav contemplated all possible tilt angles. Furthermore, most of the literature reviewed above simply

assumed that the optimal PV orientation was facing true south. The more comprehensive research was done by Khoo et al. (2014) and Yu et al. (2019), whereby they analysed the optimal PV positioning based on all possible tilt angles and surface azimuth angles.

In general, the PV modules are conventionally tilted at the site's latitude and oriented towards the equator to maximise the direct irradiance received. Nonetheless, it may not always be the optimal positioning as the optimal tilt angle and orientation depend on the local climate conditions. Khoo et al. (2014) studied three sky models, namely Liu and Jordan, Klucher, and Perez, to determine the optimal model to be used for meteorological conditions in Singapore. The models' accuracies were evaluated by comparing the estimated values with the experimental measurements in the solar farm using the normalised root mean square error (NRMSE) statistical approach. The PV panels tilted with the angles of 10 °, 20 °, 30 °, and 40 ° with the orientation at 60 °NE, and mounted vertically facing north, south, east, and west were compared. Among all the experimental results, the surfaces oriented at 60 °NE with a tilt angle of 10 ° observed the maximum irradiance. They also computed the hourly tilted irradiance (GTI) for all tilting angles and orientations using the three-year hourly measured DHI and GHI. After that, the optimal tilting angle and orientation of PV were determined by the highest annual tilted irradiances yielded for each observed year. The Perez model coefficients used were taken from Perez et al. (1990). His findings showed that three sky models gave accurate outcomes at small tilt angles, but the NRMSE would increase as the angle rose. However, among the three models, the Perez model had the least NRMSE whereby the optimal tilting angle for PV in Singapore found was in the range of 7 ° to 9 °, with the orientation of 78 ° to 88 ° North due East. This study demonstrated that the Perez model might provide better estimations for all orientations for the tropical regions.

The similar Perez model from Perez et al. (1990) was used by Yu et al. (2019) for the transposition and the optimal tilt angle and orientation determination for 837 locations in Japan. The horizontal irradiance data, typically GHI and DHI, were acquired through the MEteorological Test Data for PhotoVoltaic Version 11 system (METPV-11). Whilst the optimal orientation for various locations found was mostly towards the south, within \pm

10 °, the optimal tilt angles were in the range of 20 ° to 45 °, which the deviation from the conventional latitude tilt could be up to 15 °. The optimal tilt angle for the eastern side of Japan tended to be larger than that of the western side of Japan.

Despite Khoo et al. (2014) and Yu et al. (2019) considering all the possible surfaces orientation, the shading effect of the PV was not embraced in the PV optimisation. Jacobson and Jadhav (2018) made an assumption in the calculations using PVWatts whereby the shading factor was fixed at 0.5 %. This is not realistic as the PV shading depends on the obstruction of irradiance due to terrain, building, trees, PV front row, etc. In the subsequent subchapter, the study regarding the effect of shading on the optimal PV positioning will be discussed and reviewed.

2.2.5 Research on Shading Factor Calculation

The amount of direct solar irradiance reaching the panel surface is one of the major contributors to the output power of the PV modules, which is, in turn, greatly affected by the shading effect. According to the research done by Deline (2009), the partial shading of PV may cause a substantially greater power loss than the shaded region, and hence a precise shading computation is essential for prediction and design application. Handoko Rusiana et al. (2018) investigated the partial shadow on a 1 kWp PV system simulation using PVsyst software by modelling the PV system in West Java, Indonesia. The module tilt angle and azimuth were set at 18 ° and 0 ° (towards the North) with the solar insolation data provided by the NASA SSE. During the simulation, the shading factor table, as shown in Figure 2.1, was interpolated, which could eventually save the computation time for the software. The simulation result showed a power drop of 208 W from its nominal power (about 20.8 %) due to the shading effects. Despite the robustness of the PVsyst software, it is not ideal for research purposes as it is not an open source.

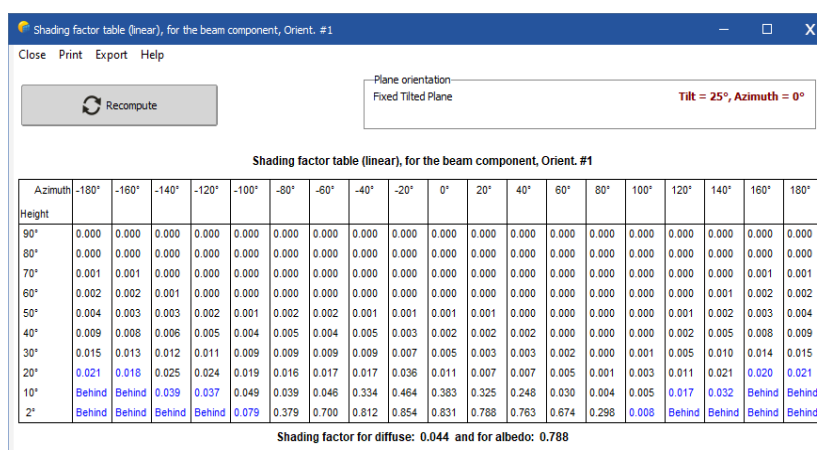


Figure 2.1: Shading Factor Table Used in PVsyst (pvsyst.com, n.d.)

In general, there are two common modelling approaches for PV module shading: the two-dimensional (2-D) geometry approach (e.g., (Quaschnig & Hanitsch, 1998; Saint-Drenan & Barbier, 2019; Varga & Mayer, 2021))) and the three-dimensional (3-D) vector approach (e.g. (Cascone et al., 2011; Melo et al., 2013; Silva et al., 2021)). Quaschnig and Hanitsch (1998) suggested various total correction factors, shading factors, energy gains, and shading losses for different tilt angles (typically 10 ° and 30 °) based on the different exploitation factors (the ratio of PV module length to row pitch, l/d). However, these parameters were only valid for middle-European sites as they were formulated from the simulation location, Berlin.

A simple inter-row shading calculation was proposed by Saint-Drenan and Barbier (2019), whereby only several PV configuration information, such as the module tilt and orientation angles, row spacing, and the module height and length, were needed. The shaded fraction calculation formula was performed using the trigonometry method and validated through the two PV plants in Delitzsch and Althen, Germany. The results demonstrated that the root mean square error (RMSE) between the proposed model and the actual implementation ranged between 7 % and 12 % for annual data and between 18 % and 32 % for time-stepped data. It might be a reasonable estimate for the inter-row shading if an infinite module row length was assumed, and the direct component of solar irradiance was affected by the shaded fraction only without considering the diffuse fraction.

Varga and Mayer (2021) determined the inter-row shading effect by calculating the obscuring angle between the top of the neighbouring row with respect to the horizontal plane. If the southern projection of the solar altitude angle was greater than the obscuring angle, the module was unshaded; else it was shaded. The Hay and Davies model for diffuse irradiance was modified to take into consideration the shading of circumsolar, sky diffuse, and albedo. They utilised the solar irradiance data on the horizontal surface from World Radiation Monitoring Centre (WRMC) to examine the shading, total energy production, total loss factor, etc., for different PV array arrangements and row spacings (1.5, 1.7, and 1.9 m). By assuming infinite module row length and panel tilt angle of 35° facing south, the total shading losses found by the proposed method (shading of all irradiance components) were about twice to five times greater than that of the simple shading calculation (shading of the direct component only). This clearly indicated the importance of accounting for the diffuse irradiance shading losses.

The combination of shading effects due to inter-row shading as well as obstacle shading was investigated by Silva et al. (2021). Instead of a simple 2-D geometric calculation for inter-row shading, a three-dimensional (3-D) vector approach was implemented. The four vertices of the PV array were given in a 3-by-1 matrix, and each vertex underwent two rotations (module tilting and orientation) and one translation displacement (adjacent row distance). A rectangular obstacle was studied, and its shadow cast on the module was cropped to calculate the shading factor. In addition, the diffuse shading factor was taken into consideration as well. The proposed method was evaluated using PV simulation software, PVsyst and SAM. The module was tilted at 30° , facing toward the true south with the inter-row spacing of 2 m. It was found that the computed shading factor for direct irradiance was in excellent alignment with the values obtained using the SAM software. On the other hand, the results generated by the PVsyst software gave great differences from the calculated value. For the diffuse shading factor, the Matlab results were well associated with the PVsyst values.

As the inter-row shading effect contributes to significant energy losses, sufficient row spacing should be established to reduce the shadow being projected from one panel to the adjacent. Elhub et al. (2012) studied the optimal

tilt angle and inter-row spacing for PV systems for different types of terrain, such as flat terrain, terrain with steps, and inclined terrain in Kuala Lumpur using Cooper's equation and Microsoft Excel Visual Basic Application (VBA) programming. The PV separation distance was calculated based on different tilt angles ranging from 10 ° to 30 °, with a step size of 5 ° and a PV length of 2 m. They found that the optimal tilt angle for Kuala Lumpur was 10 °, with 2.66 m of inter-row spacing for flat terrain. This study only focused on the shading effect without considering the surface orientation.

Al-Quraan et al. (2022) proposed a spacing multiplier factor formula that could be used for both flat and non-flat terrains to identify the optimal row spacing. Equation (2.2) and (2.3) could be used to estimate the inter-row spacing for flat and non-flat terrain, respectively, whereby the multiplier factor is given as:

$$f = \frac{\cos \theta_s}{\tan \alpha_s} \quad (2.1)$$

$$d = f \times h \quad (2.2)$$

$$d = f \times (h + \Delta h) \quad (2.3)$$

where

f = multiplier factor

d = row spacing, m

h = module height, m

Δh = height difference between two adjacent arrays, m

The formulas were then evaluated by using the case studies in the Kingdom of Saudi Arabia (flat terrain) and Dhamar, Al-Hada Yemen (non-flat terrain). The percentage errors of the optimal area between the formula and the actual installation (using software) were 11.6 % and 16 % for flat and non-flat terrain.

In general, there are two classical methods for determining the inter-row spacing of PV arrays, such as the trigonometric and empirical methods, described in Equations (2.4) and (2.5), respectively.

$$d = l \times \left(\cos\beta + \frac{\sin\beta}{\tan h_s} \right) \quad (2.4)$$

$$d = l \times \left(\cos\beta + \frac{\sin\beta}{\tan(61^\circ - \phi)} \right) \quad (2.5)$$

where

l = module length, m

β = tilt angle, °

h_s = solar height, m

Castellano et al. (2015) suggested a simple yet comprehensive method to reduce the inter-row spacing of the PV array while minimising the inter-row shadowing. For each solar hour, the shadow curves were calculated in three directions: north, east and west. Their visual representation was then computed using the trigonometric relationship based on the panel geometry and tilt angle, and a shadow envelop was identified. The derived equation was used to compare with the two conventional methods, and the results showed a 40 % reduction in the PV plant land area estimation.

The effect of partial shading on the PV modules differs depending on how they are oriented and how the shadow is cast on them. Additionally, the PV cell types and the interconnection between the cells within the modules will influence this behaviour. For a crystalline silicon module, the least performing (being shaded) cell connected in series will affect the output of a complete string, and the energy produced will be lost in terms of heat. This may create a hotspot on the shaded cell and eventually damage it. To avoid this phenomenon, integrating the bypass diode in the module will provide an alternative path for the current to flow into other substrings by omitting the particular substring with a shaded cell, as shown in Figure 2.2. A standard 60-cell crystalline silicon PV

module usually consists of three bypass diodes whereby each diode is connected to each substring of 20 cells.

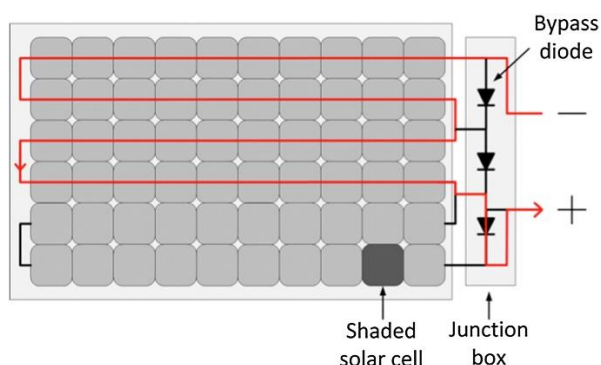


Figure 2.2: Current Flow in PV Module with One Shaded Cell (Pannebakker et al., 2017)

Although the functionality and effectiveness of the bypass diodes ensure high reliability in the PV module, it contributes to greater power loss. Several studies have investigated the PV output power when oriented in a landscape and a portrait configuration. Barreiro et al. (2011) presented a comparative analysis of the PV performance efficiency for landscape and portrait modalities using three modules: amorphous silicon, monocrystalline and polycrystalline. The test was conducted during midday (11 am – 1 pm) when the sun was at the highest point of the daily arc. The authors used the solar angle calculator tool to tilt the modules at the monthly optimal tilt angle. During the test run, the row shading at the lowest cells row was altered from 0 % to 100 % with a 20 % increment. The results showed that the electrical output efficiency could be as low as 62 % for the crystalline PV module in landscape orientation when it is 100 % shaded compared to no shading condition. For the case of portrait orientation, the efficiency loss of a crystalline module was up to 92 % when the last row of cells was fully shaded. On the other hand, the amorphous silicon module had the highest efficiency in portrait orientation, about 94 %, even when the lowest row was fully covered. This study showed that the crystalline modules in landscape orientation would be preferred over portrait orientation as two other substrings were available when one was shaded.

Oufettoul et al., (2023) carried out a similar study, but the partial shading on the PV module was due to the front PV row, which was more practical in real-life. The experiment was performed during winter when the

module shadow was the longest and most prominent. The panels were cleaned adequately throughout the testing period to avoid other environmental factors such as soil or dust depositing. The module under test (MUT) was a polycrystalline type, tilted at 31° facing towards the South, with a capacity of 3000 W. The experiment result revealed that a portrait-oriented PV module experienced significant daily energy losses exceeding 1000 Wh, while the daily energy losses in the landscape-oriented PV module were about one-quarter of the former. Although these energy losses between the two mounting orientations could not make a fair comparison as the designated dates of the investigation were different with a one-month gap due to the relative insolation, landscape mounting is still substantially superior to portrait mounting.

2.2.6 Research on Temperature Effect on the PV Performance

The performance of the PV module is greatly affected by the module operating temperature. The increment in the module operating temperature will result in a significant decrease in the output voltage and a minor rise in the output current, leading to an overall reduction in the output power produced. This is fundamentally owing to the fact that the output voltage of a solar cell is determined by its energy bandgap, whereby the bandgap is reduced when the temperature rises. On the other hand, the slight increase in the output current is due to the increased generation rate of the electron-hole pairs at higher operating temperatures. Since the overall economic viability of a project is closely tied to PV performance, it is crucial to study the influence of temperature on the proficiency of solar energy conversion.

Thong et al. (2016) investigated the effect of the different module operating temperatures on its conversion efficiency under constant ambient temperature and solar irradiance. The reason of fixing both parameters was to minimise their significant effects on PV output. The experiment setup was simple, consisting of a 10 W rated solar panel in series connection with a load resistor in a controlled condition with a constant solar irradiance of 440 W/m^2 at 38°C . The PV efficiency was calculated using the measured PV-generated voltage and current to quantify PV module behaviour under an increasing module operating temperature scenario. The efficiency graph against module operating temperature under load conditions was then plotted. The results

showed that the efficiency decreased by 23.69 % when there was a progressive rise in the PV module temperature from 38 °C to 65 °C. Nevertheless, such an experiment might be too ideal as the other atmospheric conditions, such as surrounding temperature, wind speed, and solar irradiance intensity, will eventually affect the PV efficiency.

Generally, the types of solar cell technology used will also influence the electrical performance of the PV module. For a typical PV module, it is able to convert 6 – 20 % of the solar energy into electricity while the rest is converted into heat, depending on the type of PV cell technology and the meteorologic conditions (Dubey et al., 2013). The heat generated will increase the module temperature and ultimately decrease the efficiency of the PV module's capabilities. In fact, different types of PV cell technologies react differently to the change in temperature. Adeb et al. (2019) conducted a study to evaluate the performance of three PV types, monocrystalline, polycrystalline and thin film, at different temperatures over a year in Amman, Jordan. The authors collected the weather data from the weather station near the three investigating PV systems, including all types of horizontal irradiance, wind speed and ambient temperature. Based on the collected field data, they analysed and estimated the energy yield by considering the size and area of the PV array and the efficiency of the module and inverter. After that, the estimated energy yield was compared with the actual energy yield by the three investigating PV systems. The difference between the energy yield found was assumed to be caused by the temperature effect. The study's results depicted that the annual energy yield for the three types of PV modules, monocrystalline, polycrystalline and thin film, had the deviation of 17 %, 19.5 % and 15.4 %, respectively. These differences were due to the annual average module temperature rise of 12.53 °C. Overall, this study could provide a good indication of how different PV cell technologies react to temperature variation and how much efficiency loss is due to temperature effects for different PV systems.

Other than the type of PV cell technology, the PV mounting types can significantly impact PV system performance. Different mounting systems may affect the airflow and ventilation around the PV module, which can influence the heat dissipation of the panel and the module temperature. Nordmann and Clavadetscher (2003) analysed the annual performance of 18 PV plants with

different mounting in five countries. The mounting types were categorised into the sloped roof, flat roof, free-standing and façade (integrated). All the PV modules used in the 18 plants were crystalline silicon type and tilted accordingly to the locations. Table 2.2 summarises the annual PV performance loss range and module temperature rise for the four mounting types. The PV mounted on the sloped roof would experience the largest annual loss, up to 11.3 %, due to the little air circulation between the roof and the panel, which resulted in an average module temperature rise of 55 K at 1000 W/m². A free-standing and flat roof mounting system would provide a bigger air gap from the panel, allowing airflow around the panel. This gave a better cooling mechanism to the panel, and more heat dissipation occurred. Hence, the annual loss due to the temperature effect for free-standing and flat roof mounting types was lower than for sloped roofs and façade mounting types.

Table 2.2: Range of Annual PV Performance Loss due to Temperature Effect for the Different Mounting Systems in 18 PV Plants (Nordmann and Clavadetscher, 2003)

Mounting Type	Temperature Rise (K)	Annual Loss due to Temperature Effect (%)
Sloped roof	20 - 55	1.7 - 11.3
Facade (integrated)	46 - 52	5 - 7
Free-standing	20 - 26	1.7 - 5
Flat roof	25 - 28	2.5 - 4.0

As the PV module performance is temperature-dependent, the temperature coefficients are widely used to describe the reasonably linear electrical characteristic between the PV output and its temperature. They are typically included in the datasheet of the PV module, which can be determined using the procedures listed in the international standard IEC 60891. Smith et al. (2012) tabulated the temperature coefficients for voltage, current and maximum power from over 280 PV manufacturer datasheets to study the outdoor PV module degradation rate. Table 2.3 lists all the temperature coefficient range for monocrystalline and polycrystalline silicon PV panel. The negative sign of the

coefficients indicates that the PV output, either voltage or maximum power, will decrease for every increase in the module temperature. The finding by the authors will ease the procedure of selecting the proper temperature coefficient for research purposes.

Table 2.3: List of Temperature Coefficient Range for Crystalline Silicon PV Module (Smith et al., 2012)

PV technology	Temperature coefficient of voltage, β_t (%/°C)	Temperature coefficient of current, α_t (%/°C)	Temperature coefficient of maximum power, γ (%/°C)
Mono-Si	-0.22 to -0.58	0.01 to 0.10	-0.28 to -0.56
Poly-Si	-0.18 to -0.55	0.018 to 0.12	-0.34 to -0.54

Even though several works of literature highlighted that the temperature coefficients given in the datasheets may not always be precise (Figgis and Abdallah, 2019; Paudyal and Imenes, 2021), they could still be helpful for estimation analysis.

In the absence of a temperature sensor directly measuring the PV module temperature, a temperature model for the PV system can be used to predict the temperature under different climatic conditions and how it will impact the PV performance over time. The Ross coefficient model is one of the simplest and most commonly used temperature models. It was developed by Ross (1976), who pointed out that as the in-plane irradiance rises, the module operating temperature would increase above the ambient temperature. Olukan and Emziane (2014) criticised the Ross coefficient model would underestimate the PV module temperature, especially in high-temperature scenarios, after analysing it with the actual case. Lai and Lim (2019) proposed overall and time-specific Ross coefficients by assessing the direct PV temperature measurement and deriving the coefficients based on the measurement. The authors conducted two setups at Bukit Kayu Hitam and Kajang, using monocrystalline silicon PV with free-standing mounting and polycrystalline silicon PV mounted on the metal deck, respectively. Lai and Lim's derived Ross coefficients were tabulated as in Table 2.4.

Table 2.4: Overall and Time-specific Ross Coefficients for Different Mounting Types (Lai and Lim, 2019)

Mounting Type	Overall Ross Coefficient (°C/(W/m²))	Time-specific Ross coefficient (°C/(W/m²))
Free-standing	0.0216	0.0085 – 0.0286
Metal deck (10 cm air gap)	0.0264	0.004 – 0.032

After developing the Ross coefficients, the authors utilised the Mean Absolute Error (MAE) and Root Mean Square Error (RMSE) to compute the difference between the estimated and measured module temperature. The evaluation showed that the overall and time-specific Ross coefficients had the RSME of about 3.25 °C and 2.5 °C, respectively. Since the RSMEs for both Ross coefficients were relatively small, the derived overall Ross coefficient would be easier to implement as the time factor could be omitted, simplifying the calculation in the study.

Skoplaki et al. (2008) adapted various Ross coefficients for different mounting types (as in Table 2.5) from the data provided by Nordmann and Clavadetscher (2003). It was apparent that the Ross coefficient of the free-standing mounting type derived by Lai and Lim (2019) was approximately the same as that in Table 2.5. Based on the coefficients in Table 2.5, the authors developed the normalised mounting coefficients (a reference to free-standing) and integrated them into a modified PV module operating temperature model. Nonetheless, the authors did not validate the proposed temperature model using the actual field data; thus, the model's accuracy was doubtful.

Table 2.5: Ross Coefficients for Different Mounting Types (Skoplaki et al., 2008)

Mounting Type	Ross Coefficient (°C/(W/m²))
Flat roof	0.026
Free-standing	0.021
Well-cooled inclined roof	0.020
Poorly cooled inclined roof	0.034
Highly integrated, inefficiently ventilated inclined roof	0.056
Transparent, building integrated	0.046
Opaque, building integrated	0.054

Aoun (2022) conducted a study comparing and evaluating the accuracy of five temperature models: Ross, Sandia, Thermal, Normal Operating Cell Temperature (NOCT) and Skoplaki models. The experiment days were selected from two different seasonal months: January (cold) and July (hot). The actual instantaneous module temperature of the specified days was compared to the estimated one using the five temperature models. The RSME for each model was computed to appraise the accuracy. During the winter month, the NOCT, Sandia, and Thermal models overestimated the PV module temperature, while the module temperature estimated using the Skoplaki model was slightly exaggerated compared to the empirical value. Despite its simplicity, the Ross model produced an excellent fitting curve with the actual data. On the other hand, the Sandia, Ross, and Skoplaki models achieved the best results with the actual measurement during the summer month. The NOCT model performed even worse in the hot than in the cold season. Besides that, the module temperature estimated by the Thermal model was less affected by the weather or seasonal change. In addition, the scatter plot of the estimated against actual module temperature, as shown in Figure 2.3, showed that the deviation between the actual and estimated value by the five temperature models was small in the hot months but was the opposite in the cold month. Overall, the author

summarised that the accuracy of all five models was close to each other throughout the years, with the range of RSME between 0.45 and 5.7 °C. In the tropical area, the surrounding temperature remains relatively warm throughout the year, and hence any of the temperature models will eventually produce the same estimation results.

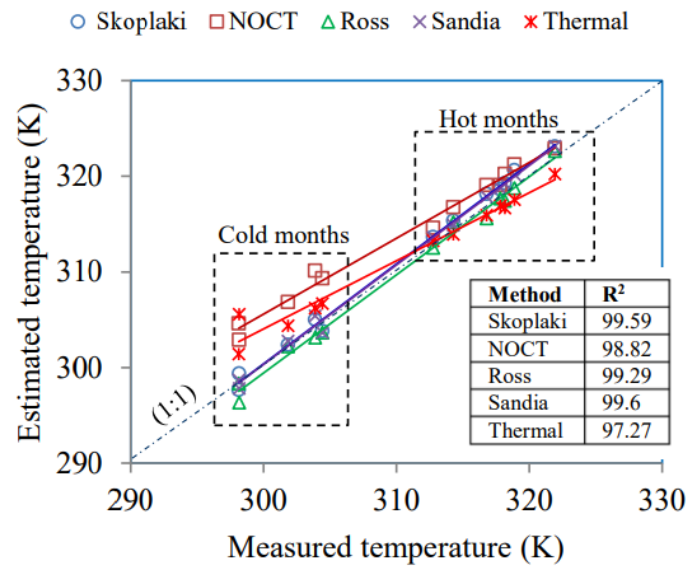


Figure 2.3: Scatter Plots between the Measured and Estimated Module Temperature (Aoun, 2022)

2.3 Summary

Table 2.6 summarises the research on determining the optimal tilt angle and orientation for different latitudes and methods used, while Table 2.7 summarises the research on determining the shading factor and optimal row spacing. Table 2.8 summarises temperature effect on the PV performance and the temperature model.

Table 2.6: Details of the Methods/Models Used to Determine the Optimal Tilt Angle and Orientation

Papers	Location	Consideration		Optimal		Irradiance Data	Software/ Approach	Method/model	Shading Consideration
		Tilting angle	Orientation	Tilting angle	Orientation				
Khoo et al., 2014	Singapore (1.37 °N, 103.75 °E).	10 ° - 40 ° & 90 °	60 °NE & 0 °N, 180 °S, 90 °E, 270 °W	10 ° (7 - 9° *)	East (North due East, 78 – 88 °NE *)	Three-year measured GHI & GTI data	-	Sky models (Perez et al. model*)	-
Fadaeenejad et al., 2015	Sarawak (1.44 °N, 110.074 °E), Sabah (5.32 °N, 115.60 °E), & Selangor (2.95 °N, 101.54 °E).	0 °, 5 °, 10 °, 15 °	180 °S	0 °, 5 °, 0 °	180 °S (by default)	NASA SSE	iHOGA	Liu and Jordan model	-
Yu et al., 2019	837 locations in Japan	Latitude (Conventional)	Towards equator (Conventional)	20 ° - 40 ° (σ = 15 °)	± 10 ° of true S Western - Eastern	METPV-11	-	Perez et al. model	-
Matius et al., 2021	Liogu Ku Silou-Silou, Sabah (6.2514 °N, 116.4643°E)	-	0 °N, 180 °S	8.05 ° (yearly)	South (yearly)	17 sets of daily data with increments of 30 min	Excel	Liu and Jordan, Koronakis, Badescu, Tian models	-
				24 ° (Jan - Mar, Sept-Dec)	South (Jan - Mar, Sept-Dec)				
				17 ° (Apr - Aug)	North (Apr - Aug)				

Table 2.6 (Continued)

Jacobson and Jadhav, 2018	Kuala Lumpur, Malaysia (3.12 °N, 101.55 °E).	-	180 °S	1 °	180 °S (by default)	ASHRAE IWEC 1.1 & SWERA	PVWatts	-	Yes (0.5 %)
Khatib et al., 2015	Kuala Lumpur, Johor Bharu, Ipoh, Kuching, & Alor Setar	-	-	Wet season: 15 ° - 23 ° Dry season: 0 °	-	Historical data (1975–2005) from SERI, UKM	-	Liu and Jordan model	-
Elhassan et al., 2011	Kuala Lumpur	15 °, 20 °, 30 °	0 °N, 180 °S, 90 °E, 270 °W	15 °	180 °S	One-year recorded weather data	Matlab & PVSYS-50	-	-
Mamun et al., 2017	Eight cities in Bangladesh	-	-	25 ° - 30 °	-	-	SAM software	-	-
Hailu and Fung, 2019	Greater Toronto Area (GTA), Canada (43.7 °N, -79.2 °E)	0 ° - 90 ° (Step of 1 °)	180 °S ± 30 °	Isotropic: 37 ° - 44 ° Anisotropic: 46 ° - 47 °	180 °S	<i>METEONORM</i> v.7	Matlab	Four isotropic and four anisotropic models	-
Abdullahi et al., 2020	Kano, Nigeria (12.00 °N, 8.5920 °E)	0 ° - 90 °	-	12.05 ° (equal to latitude)	-	NiMet	EES	Liu and Jordan model	-

Table 2.7: Details of the Methods/Models Used to Determine the Shading Factor and Row Spacing

Papers	Location	Method/ Approach	Software	Shading Type	Assumption/ Consideration	Effect of Shading		Irradiance Data	Optimal		Row spacing
									Tilt	Orientation	
Varga and Mayer, 2021	Budapest, Hungary	2D geometry approach (Shading factor: 0 or 1)	-	Inter-row shading	Infinite module row length	On direct, diffuse, and ground reflected	World Radiation Monitoring Centre (WRMC)	35 ° (assumed)	South (assumed)	1.5 m, 1.7 m, 1.9 m (study loss factor)	
Handoko Rusiana et al., 2018	West Java, Indonesia (6.884 °S, 107.54 °E)	Shading factor table	PVSyst.	-	-	Direct	NASA SSE	18 ° (assumed)	North (assumed)	-	
Silva et al., 2021	Mar del Plata, Argentina (38 °S, 57.5 °W)	3D Matrices/Vector approach, Shading factor table	Matlab, SAM, PVsyst	Inter-row shading, Obstacle shadow	Rectangular obstacle	Direct, diffuse	-	30 ° (assumed)	North (assumed)	2 m	
Al-Quraan et al., 2022	Kingdom of Saudi Arabia (KSA) Dhamar, Al-Hada, Yemen *	2D geometry approach	-	Inter-row shading	Flat terrain & non-flat terrain*	-	-	15 °, 13 °* (validation)	-	$\frac{\cos \theta_s}{\tan \alpha_s} \times h$ $\frac{\cos \theta_s}{\tan \alpha_s} \times (h \pm \Delta h)$ *	
Saint-Drenan and Barbier, 2019	Delitzsch (51.51 °N, 12.29 °E) and Althen (51.35 °N, 12.52 °E), Germany	2D geometry approach	-	Inter-row shading	Infinite module row length	Direct	Measurement data from two sites	25 ° (validation)	South (validation)	2.4 m, 2.7 m	

Table 2.7 (Continued)

Quaschnig and Hanitsch, 1998	Berlin, Germany		2D geometry approach	-	Inter-row shading	Only valid for middle-European sites	-	-	10°, 30°	-	-
Elhub et al., 2012	Kuala Lumpur (3.16 ° N, 101.71 ° E).		Cooper's equation	Excel (VBA programming)	Inter-row shading	-	-	-	10°	-	Yes (Row pitch: 2.66 m; PV Length: 2 m)
Castellano et al., 2015	South of Spain (37.09 ° N, -2.63 ° E).		Novel shading model	-	Inter-row shading	Tilt angles: 15°, 40°, 45°, & 60°	-	-	-	-	40 % improvement compared to classical approach

Table 2.8: Summary of the Temperature Effect on the PV Performance and the Temperature Model

Papers	Location	Study Scope	Method/ Approach	PV Types	Effect of Temperature	Input Data	PV Positioning	
							Tilt	Orientation
Thong et al. (2016)	-	PV performance with different module operating temperature	Compute the efficiency of PV module under different temperature	-	Efficiency dropped by 23.69 % with 27 °C rise in module operating temperature.	-	-	-
Adeeb et al. 2019)	Amman, Jordan	PV performance using different solar cell technology	Compute the difference between actual and estimated energy yield	s-Mono, s-Poly, Thin-film	Annual energy loss: s-Mono: 17 % s-Poly: 19.5% S-Thin-film: 15.4 %	Measured horizontal irradiance, weather condition, and measured annual energy yield	11 °	South
Nordmann and Clavadetscher (2003)	18 PV sites in Austria, Japan, Germany, Italy, Switzerland	PV performance using different mounting system	Compute the annual loss due to temperature effect	Crystalline silicon	As shown in Table XX	Actual field data	According to the site location	-
Smith et al. (2012)	Golden, Colorado	PV module degradation	-	s-Mono, s-Poly	< 0.5%/year degradation (not in focus)	Measured values for FF, I _{max} , I _{sc} , P _{max} , V _{max} , and Voc	40° (±1°)	South (±2°)
Lai and Lim (2019)	Bukit Kayu Hitam and Kajang, Malaysia	Ross coefficient derivation	Compute the gradient of temperature against in-plane irradiance	s-Mono, s-Poly	RMSE: 2.5 -3.25 °C	In-plane irradiance, actual module temperature	10 °	South
Skoplaki et al. (2008)	-	Skoplaki temperature model derivation	Skoplaki model	-	% Diff: 0 - 13.9 %	-	-	-
Aoun (2022)	Saharan Environment, Adrar, Algeria	Evaluate the accuracy of temperature model	Ross, Thermal, Skoplaki, NOCT, Sandia models	s-Mono	RMSE: 0.45 -5.7 °C	In-plane irradiance, weather data, actual module temperature	28 °	South

CHAPTER 3

METHODOLOGY AND WORK PLAN

3.1 Introduction

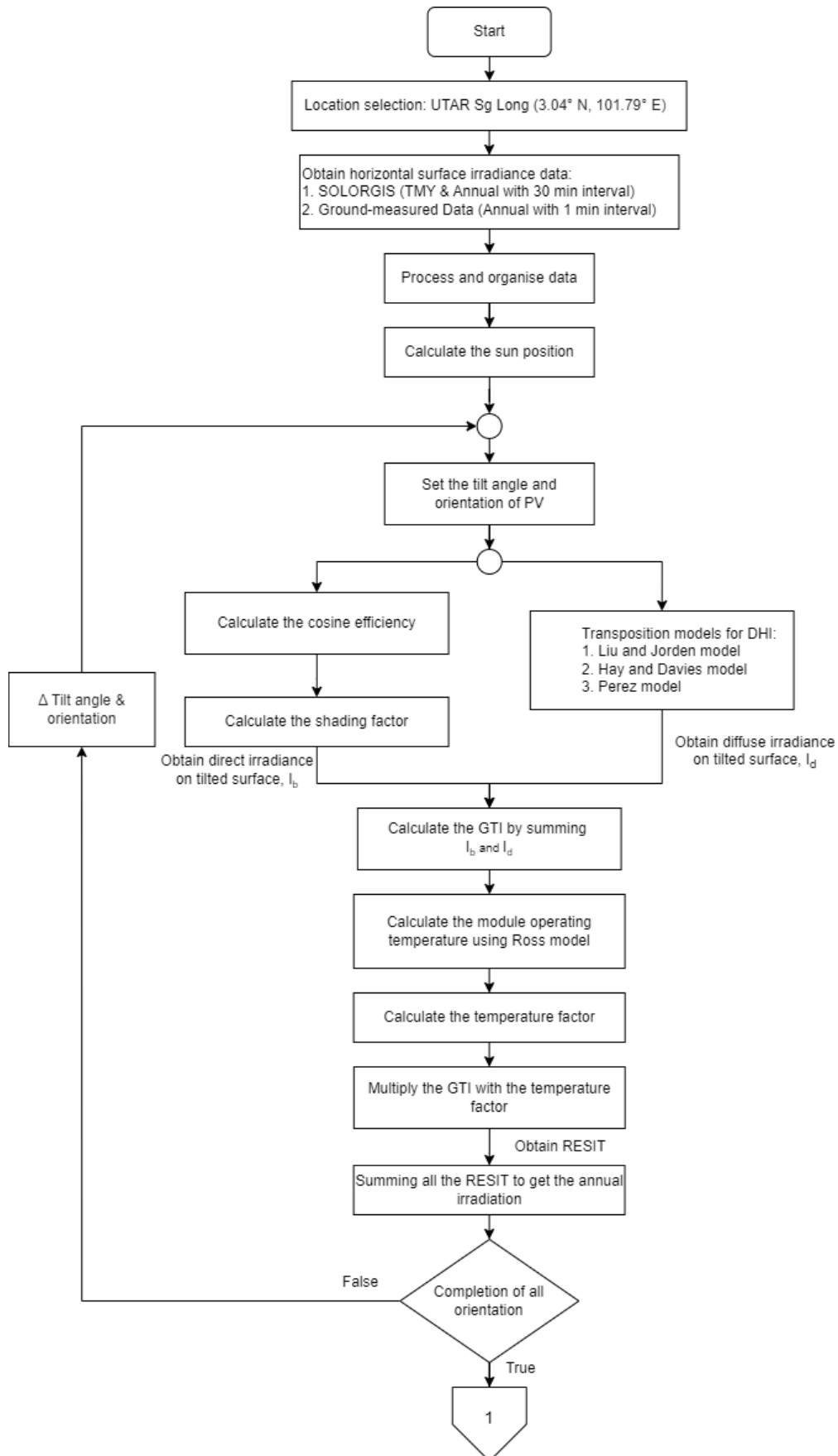
This chapter explains the procedures for determining the optimal PV system tilt angle and orientation. The location chosen for the study is the University of Tunku Abdul Rahman (UTAR), Sg Long Campus in Kajang, Selangor (3.0396 °N, 101.7942 °E).

Three transposition sky models are implemented to convert the horizontal irradiance into tilted irradiance. The shading and temperature effects are also considered in the computation. In addition, the characteristic of inter-row shading for different pitch distances and panel configurations will be analysed. A simple Ross coefficient model is utilised to estimate the module operating temperature, and its impact on the PV performance will be investigated. Most of the computations of the study rely on the functions in the pvlib python library contributed by F. Holmgren et al. (2018). This project will fully utilise python programming for data processing and computation.

3.2 Flowchart of Work

Figure 3.1 illustrates the flowchart of this project as an overall concept and guideline to perform.

The study begins with choosing a location for investigation: UTAR Sg Long. Two types of horizontal surface irradiance data, namely Solargis (satellite-derived solar irradiance) and ground-measured data, are utilised as the input for the tilted irradiance computation. Next, the hourly solar position is calculated, and the hourly direct and diffuse components on the tilted surface are computed using three transposition models and considering the shading effect. After obtaining the in-plane solar irradiance, the module operating temperature is estimated using the Ross coefficient model. The module temperature is then used to calculate the temperature factor, which will multiply with the global tilted irradiance to obtain the reduced equivalent solar irradiance due to temperature (RESIT). The summation of all interval RESIT gives the annual tilted irradiation. The steps are repeated for all possible orientations and tilt angles. The optimal tilting angle and orientation of PV are determined from the highest tilted irradiation yielded. Besides, the characteristics of optimal angles at various conditions will be analysed.



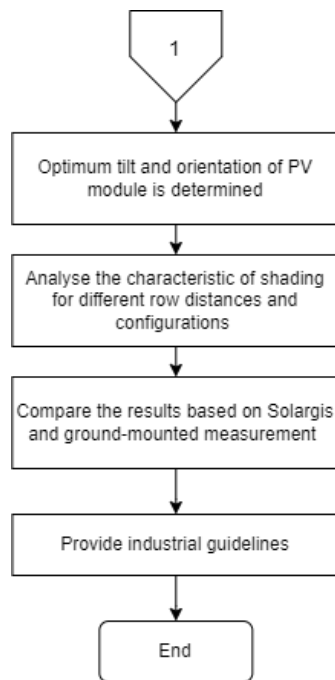


Figure 3.1: Work Flowchart

3.3 Irradiance Data

To determine the optimal tilt angle and orientation of the PV system, GHI, DNI, and DHI are needed to perform the transposition. The definitions of the solar irradiance type can refer to the literature review subsection 2.2.2. The studied location's irradiance data are obtained from satellite-derived data and ground-based solar irradiance measurements.

3.3.1 Satellite-derived Data

Satellite-derived data is the estimation of solar irradiance based on satellite images. The estimation can be done using two empirical, physical or statistical methods. The former is based on the radiative processes analysis when sun ray travels through the earth's atmosphere; the latter relies on the relationship between earth surface measurement and satellite information (Goswami, 2015). There are numerous satellite-derived solar resource databases such as Meteonorm, Solargis, PVGIS, SolarAnywhere, etc. In this study, Solargis is chosen as the empirical data for computation.

Solargis offers a reliable and accurate database due to its high satellite footprint resolution (250 m × 250 m spatial resolution), which can adequately describe normal and extreme weather conditions (Solargis, 2022). It also delivers the solution for design optimisation and historical performance review evaluation by providing the Typical Meteorological Year (TMY) and time series data for any project site.

A TMY data is constructed from summarised information of multiple years time series, reflecting a particular location's typical climate. A TMY P50 dataset is used for the study, whereby extreme weather conditions are not considered. The summarised period is ranged from the year 1999 to the year 2021 with an hourly time step.

Another historical time series data with a 30-minute time step (from 1st January 1999 to 31st January 2022) is compared with ground-based measurement for determining the optimal tilt angle and orientation.

3.3.2 Ground-based Solar Irradiance Measurement

A pyranometer and a pyrheliometer are commonly used devices for measuring solar radiation. Due to its hemispherical field of view, the pyranometer measures the total solar irradiance (typically direct plus diffuse). On the other hand, the pyrheliometer can measure the beam components only due to its limited view of about 5° .

The diffuse irradiance can be measured by shading the pyranometer using a shaded ring or disc, as shown in Figure 3.2. The difference between the measured total and diffuse irradiances is computed to estimate the beam radiation alternatively.

One year of irradiance measurement is performed from 1st January 2020 to 31st December 2020 on the University of Tunku Abdul Rahman (UTAR), Sg Long Campus rooftop. The sensor's placement on the rooftop is free from any obstructions, and therefore the shading due to the surrounding building or vegetation can be avoided throughout the year. The data collected are sampled and logged at one-minute intervals.

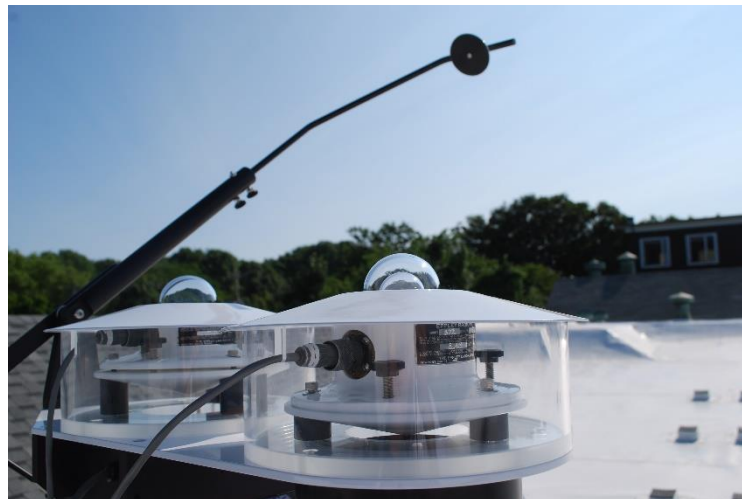


Figure 3.2: Irradiance Measurement on Horizontal Surface. (eppleylab.com, 2022)

3.4 Modelling of Solar Irradiance on Tilted Surfaces

The total solar insolation received by the panel comprises the direct component, the diffuse component, and the ground-reflected component. The transposition models are used to convert the horizontal irradiance (GHI) to the tilted irradiance (GTI). The direct component of the insolation on a slanted surface can be computed using geometric relations. In contrast, the conversion for diffuse component needs to utilise the sky models, such as Liu and Jordan, Hay and Davies and Perez models. The ground-reflected component, however, is neglected in the study.

3.4.1 Modelling of Tilted Direct Irradiance

Considering the cosine efficiency and the effect of shading, the direct irradiance on a tilted surface is given as:

$$I_b = DNI \times \cos\theta \times (1 - f_s) \quad (3.1)$$

where

I_b = direct irradiance on a tilted surface, W/m^2

DNI = direct normal irradiance on a horizontal surface, W/m^2

$\cos\theta$ = cosine efficiency

f_s = shading factor

3.4.1.1 Definition of Cosine Efficiency

Cosine efficiency, also known as the cosine effect, refers to the reduction in the incident energy due to the cosine angle (angle of incidence, AOI) formed between the normal line of the PV module surface and the solar radiation vector. As the angle of incidence increases, more solar radiation is reflected from the PV module surface. This eventually decreases the output power generation of the PV system.

The AOI can be calculated by determining the dot product of the solar radiation vector and the normal vector of the PV module surface, divided by the product of the magnitude of both vectors as follows:

$$\cos \theta = \frac{\vec{I} \cdot \vec{N}}{|\vec{I}| |\vec{N}|} \quad (3.2)$$

where

\vec{I} = solar radiation vector

\vec{N} = normal vector of the PV module surface

By solving Equation (3.2), the final expression of the cosine effect equation is given as follows (Iqbal, 1983):

$$\cos \theta = \cos \beta \cos \theta_z + \sin \beta \sin \theta_z \cos(\theta_s - \theta_p) \quad (3.3)$$

where

θ_z = solar zenith angle, °

θ_p = PV azimuth angle, °

3.4.1.2 Shading Factor Calculation

Several parameters are required in deriving the shading factor, such as the solar altitude angle and azimuth angle (α_s, θ_s), the module length and height (l, h), the module tilt and azimuth angle (β, θ_p), and the inter-row spacing (d). The solar position can be obtained through Equation (2.1), (2.2) and (2.3).

The shading factor of the PV module is computed by a simple 2D geometrical approach (Saint-Drenan and Barbier, 2019). The solar farm with parallel rows of infinite module row length on flat terrain is assumed to simplify the geometric calculation. As a result, the module shading behaviour is consistent throughout the row, and the analysis can be performed at any PV array cross-section. In other words, the shading difference at the start and end of each row is neglected. It can provide an acceptable estimation for lengthy rows in a large-scale solar farm (LSS) but may lead to significant discrepancies for small-scale PV installations.

Figure 3.3 illustrates a 3D representation of the inter-row shading and a red rectangular plane consisting of a vector pointing in the sun's direction and a normal to the horizontal flat terrain. The red rectangular plane is then drawn out, as shown in Figure 3.4, with two thick, blue lines marked by segments [AB]

and [DG] representing the two module rows. The red triangle in Figure 3.4 shows the shadow projection of point A on the second-row module at point F and on the ground at point E.

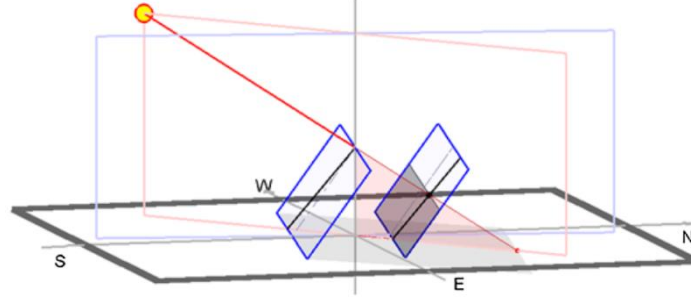


Figure 3.3: 3D Representation of the Inter-row Shading (Saint-Drenan and Barbier, 2019)

Assuming an infinite module row length, the ratio of DF to DG defines the percentage of the shaded region on the panel area, which is also given as the shading factor, f_s . Since the module length is the same for each row ($DG = BA$), the f_s is equal to the ratio of DF to BA . This ratio can be then determined by performing the theorem of the similar triangle on triangles (DEF) and (BEA) ($DF/BA = DE/BE$). Therefore, the shading factor is given as follows:

$$\text{shading factor, } f_s = \frac{DF}{DG} = \frac{DF}{BA} = \frac{DE}{BE} = \frac{CE - CD}{BC + CE} \quad (3.4)$$

The lengths CE, CD, and BC can be computed by simple trigonometry formulas, which are shown in Figure 3.4 and Figure 3.5. By substituting all these lengths into Equation (3.4), the shading factor can be expressed as follows:

$$f = \begin{cases} \frac{\left| \frac{l \sin \beta}{\tan \alpha_s} \right| - \left| \frac{d}{\cos(\theta_s - \theta_p)} \right|}{\left| l \cos \beta / \cos(\theta_s - \theta_p) \right| + \left| l \sin \beta / \tan \alpha_s \right|} & \text{if } |\alpha_s - \beta| < \frac{\pi}{2} \\ 0 & \text{if } |\alpha_s - \beta| \geq \frac{\pi}{2} \end{cases} \quad (3.5)$$

A negative shading factor may be obtained by using Equation (3.5), which indicates zero shading on the PV module.

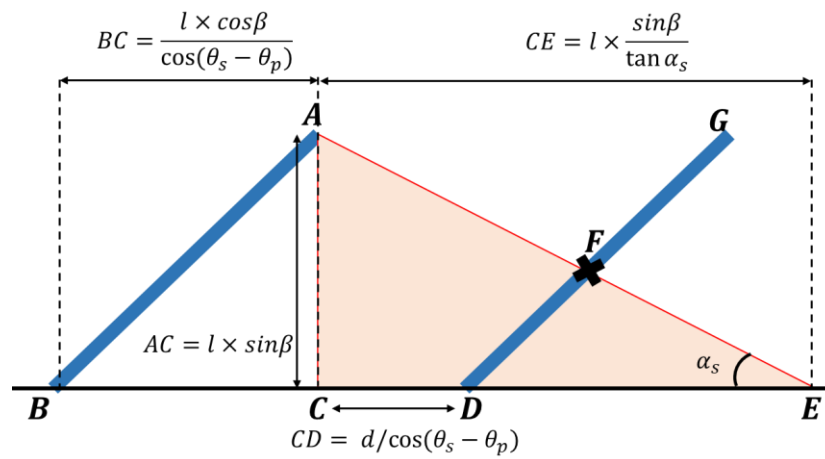


Figure 3.4: Rectangular Plane Including the Shadow Projection (Saint-Drenan and Barbier, 2019)

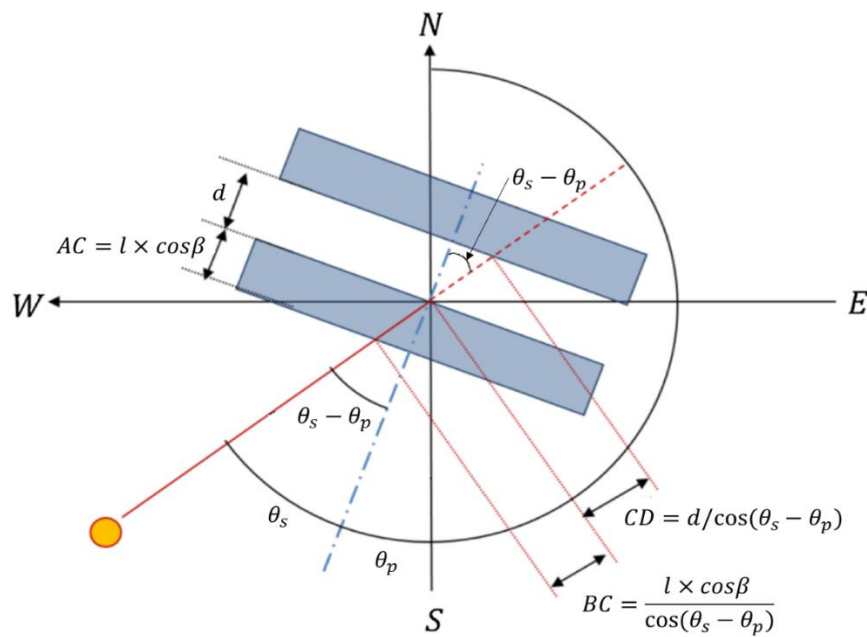


Figure 3.5: Top View of the 3D Representation of Inter-row Shading (Saint-Drenan and Barbier, 2019)

3.4.2 Modelling of Tilted Diffuse Irradiance

3.4.2.1 Liu and Jordan Model

Liu and Jordan model is a simple transposition model whereby the diffuse sky component is assumed to be isotropic (Liu and Jordan, 1961). It can be calculated as follows:

$$I_d = DHI \left(\frac{\cos\beta + 1}{2} \right) \quad (3.6)$$

where

DHI = Diffuse horizontal irradiance, W/m^2

I_d = Tilted diffuse irradiance, W/m^2

Despite its simplicity, the underlying assumption of uniform diffuse sky radiation over the sky dome is not always correct.

3.4.2.2 Hay and Davies Model

Hay and Davies (1980) suggested a model by dividing the diffuse irradiance into circumsolar and isotropic components. In addition, the diffuse components are considered to be in the same direction as direct irradiance and horizon brightening is neglected. The following equation shows the diffuse irradiance on a tilted surface using the Hay and Davies model:

$$I_d = DHI \left(A_i R_b + (1 - A_i) \left(\frac{\cos\beta + 1}{2} \right) \right) \quad (3.7)$$

$$R_b = \frac{\cos(AOI)}{\cos\theta_z} \quad (3.8)$$

$$A_i = \frac{DNI}{I_0} \quad (3.9)$$

where

AOI = angle of incidence, $^{\circ}$

A_i = Anisotropic index

I_0 = Extraterrestrial radiation, W/m^2

Nevertheless, tilted diffuse irradiance estimated by Hay and Davies model may have slightly higher predictions as its complexity is not much higher than the isotropic model (Duffie and Beckman, 2013).

3.4.2.3 Perez Model

The model proposed by Perez et al. (1990) is derived from an exhaustive analysis of the sky diffuse components. It divides the diffuse irradiance into isotropic, circumsolar, and horizon brightening.

$$I_d = DHI \left((1 - F_1) \left(\frac{\cos \beta + 1}{2} \right) + F_1 \frac{a}{b} + F_2 \sin \beta \right) \quad (3.10)$$

where

F_1 = circumsolar brightness coefficient

F_2 = horizon brightness coefficient

The incident angles of the circumsolar radiation cone on the inclined and horizontal surfaces are represented by the a and b expressions, whereby they are defined as

$$a = \max(0, \cos AOI), \quad b = \max(0.9962, \cos \theta_z) \quad (3.11)$$

The sky brightness index, Δ and clearness index, ε are defined as

$$\Delta = m \frac{DNI}{I_0} \quad (3.12)$$

$$\varepsilon = \frac{5.535 \times 10^{-6} \theta_z^3 + \frac{DNI+DHI}{DHI}}{5.535 \times 10^{-6} \theta_z^3 + 1} \quad (3.13)$$

where

m = air mass

The F1 and F2 brightness coefficients are given as:

$$F_1 = \max \left[0, \left(f_{11} + \Delta f_{12} + \frac{\pi \theta_z}{180} f_{13} \right) \right] \quad (3.14)$$

$$F_2 = f_{21} + \Delta f_{22} + \frac{\pi \theta_z}{180} f_{23} \quad (3.15)$$

where

f_{ij} = coefficients of Perez model

The Perez model coefficients used for the study are taken from Perez et al. (1990), as shown in Figure 3.6.

Range of ε	f_{11}	f_{12}	f_{13}	f_{21}	f_{22}	f_{23}
1.000–1.065	−0.008	0.588	−0.062	−0.060	0.072	−0.022
1.065–1.230	0.130	0.683	−0.151	−0.019	0.066	−0.029
1.230–1.500	0.330	0.487	−0.221	0.055	−0.064	−0.026
1.500–1.950	0.568	0.187	−0.295	0.109	−0.152	0.014
1.950–2.800	0.873	−0.392	−0.362	0.226	−0.462	0.001
2.800–4.500	1.132	−1.237	−0.412	0.288	−0.823	0.056
4.500–6.200	1.060	−1.600	−0.359	0.264	−1.127	0.131
6.200–∞	0.678	−0.327	−0.250	0.156	−1.377	0.251

Figure 3.6: Coefficients of Perez Model (Perez et al., 1990)

3.5 Modelling of Reduced Equivalent Solar Irradiance (RESI)

The partial shading on the PV modules may lead to higher power loss due to bypass diodes, depending on how they are oriented and how the shadow is cast on them. The temperature effect is another factor that will influence the PV output efficiency. The higher the module operating temperature, the lower the output power generated by the PV system. Therefore, it is crucial to determine how much power is lost due to the shading effect considering the bypass diode and the temperature effect. This study will focus on the impact of the temperature and bypass diode on the PV performance. The other factors contributing to the PV power loss, such as module array mismatch loss, module quality loss, inverter loss, and ohmic wiring loss, will be neglected. By isolating these two parameters, optimising the PV system design and improving its overall efficiency will be easier. Since the output power of a PV system is directly related to the amount of in-plane solar irradiance, the reduced equivalent-solar irradiance can be used to represent the net PV output power.

3.5.1 Reduced Equivalent Solar Irradiance due to Shading–Bypass Diode (RESIS)

In designing a PV system, there are various panel configurations to consider. The PV panels can be oriented in landscape or portrait and even be stacked in multiple layers to yield more solar power. This study will investigate six different types of panel configurations to determine their impact on PV performance. They are landscape, landscape with two stacked, landscape with three stacked, landscape with four stacked, portrait, and portrait with two stacked. Figure 3.7 shows the effect of partial shading for different panel configurations.

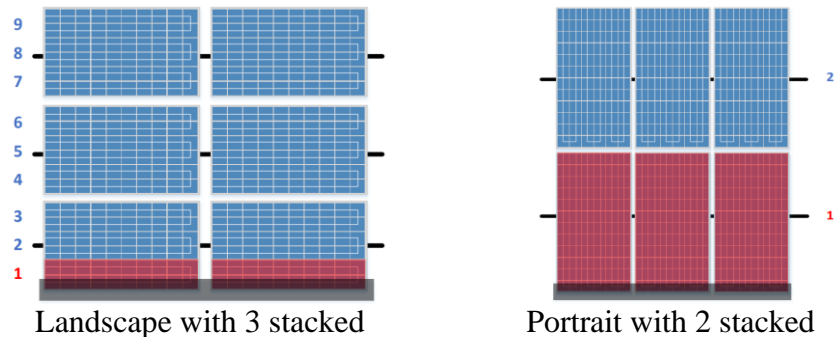


Figure 3.7: Effect of Partial Shading for Different Panel Configurations (Deline et al., 2014)

3.5.2 Reduced Equivalent Solar Irradiance due to Temperature (RESIT)

Estimating the PV module temperature is essential in investigating its impact on PV performance. Numerous studies have been conducted to validate the temperature model's accuracy. Aoun (2022) suggested that the estimation value of temperature models was as close to each other in the hot season. Despite its simplicity, the Ross model gave excellent curve fitting with the actual data during winter and summer. Therefore, this paper uses the Ross coefficient model to predict the module operating temperature.

3.5.2.1 Ross Coefficient Model

Ross (1976) developed an explicit linear equation to predict the module operating temperature, as shown in Equation (3.16), considering several factors, including in-plane solar irradiance, ambient temperature, and Ross coefficient. Assuming the PV mounting system is free-standing, the Ross coefficient value used is $0.0.21 \text{ } ^\circ\text{C}/(\text{W}/\text{m}^2)$ (Skoplaki et al., 2008).

$$t_m = t_a + k_{Ross} \times I_r \quad (3.16)$$

where

t_m = PV module operating temperature, $^\circ\text{C}$

t_a = ambient temperature, $^\circ\text{C}$

k_{Ross} = Ross coefficient, $^\circ\text{C}/(\text{W}/\text{m}^2)$

I_r = in-plane solar irradiance, W/m^2

3.5.2.2 Temperature Factor Calculation

The effect of temperature on the maximum PV output power, P_{max} , can be described by the following equation:

$$P_{max2} = P_{max1}[1 + \gamma(t_m - 25)] \quad (3.17)$$

$$f_{temp} = [1 + \gamma(t_m - 25)] \quad (3.18)$$

where

P_{max2} = PV maximum output power after considering temperature effect, W

P_{max1} = PV maximum output power before considering temperature effect, W

f_{temp} = temperature factor

γ = temperature coefficient of maximum power, %/°C

As this study focuses on the crystalline silicon PV technology, the temperature coefficient of maximum power, γ , is assumed to be -0.36 %/°C. Once the temperature factor is computed, it will be multiplied by the in-plane solar irradiance to produce the reduced equivalent solar irradiance due to temperature (RESIT).

3.6 Determining the Optimal Tilt Angle and Orientation

The different time step is used to calculate the tilted irradiance for the different type of solar irradiance data. The time step for Solargis TMY data is in 1-hour intervals as provided, while that of the Solargis Time Series data and ground-based measurement is at every 30-minute interval. The hourly and 30-minute interval tilted irradiance is calculated using Python programming for all possible orientations (range from 0 ° to 360 ° with 1 ° step interval) with tilt angles ranging from 0 ° to 15 °. The tilt angle is limited to 15 ° as the optimal tilt angle presented by most of the studies in Malaysia were below that particular value. Hence, this eventually saves computation time.

The pvlib python library is used in the study due to various functions provided that substantially simplify the PV module simulation. All the transposition model calculations, such as Liu and Jordan, Hay and Davies and

Perez models in the study, will utilise the built-in functions in pvlib. The shading losses, the cosine efficiency on direct components, the Ross coefficient model and the temperature factor calculation will be explicitly programmed, as they are not provided in the library.

After obtaining the tilted irradiance for each time interval, the annual tilted insolation is calculated by adding the tilted irradiance for each tilt angle and orientation for a year. The optimal orientation and tilt angle are then determined by yielding the highest annual tilted insolation.

The analysis of shading characteristic with different row distances and panel configurations are conducted. The pitch-distance-to-PV-length ratio (DL ratio) will manipulate the pitch row distance. The DL ratio ranging from 1.0 to 2.0 will be considered, and the effect of inter-row shading will be analysed. The relationship between the shading factor, panel landscape, and portrait configuration will also be studied.

The results of this study based on Solargis data and ground-based measurement data will be compared and analysed. These results will give the industry a guideline to install at optimal orientation and tilting angles to yield the maximum PV output considering shading loss and temperature effect.

3.7 Statistical Evaluation

In order to quantify the amount of loss due to shading and temperature effect, several statistical metrics have been utilised. These metrics include the mean absolute difference (MAD), root mean square difference (RMSD), mean absolute percentage difference (MAPD), and highest absolute percentage difference (HAPD). The formulas are given as follows:

$$MAD = \frac{1}{N} \sum_{n=1}^N X_{n,1} - X_{n,2} \quad (3.19)$$

$$RMSD = \sqrt{\frac{1}{N} \sum_{n=1}^N (X_{n,1} - X_{n,2})^2} \quad (3.20)$$

$$MAPD = \frac{1}{N} \sum_{n=1}^N \frac{|X_{n,1} - X_{n,2}|}{X_{n,1}} \times 100\% \quad (3.21)$$

$$HAPD = \max \left\{ \frac{|X_{n,1} - X_{n,2}|}{X_{n,1}} \times 100\% \right\}_{n=1}^N \quad (3.22)$$

where

MAD = mean absolute difference

RMSD = root mean square difference

MAPD = mean absolute percentage difference, %

HAPD = highest absolute percentage difference, %

$X_{n,1}$ = entries of data set 1 or reference set

$X_{n,2}$ = entries of data set 2

The RMSD and MAPD are specifically used to determine the deviation between two data sets. On the other hand, the HAPD provides insights into the worst-case scenarios and represents the maximum deviation between two data groups. Using these statistical metrics makes it possible to obtain a more comprehensive understanding of the amount of loss due to shading and temperature effects in a given scenario.

3.8 Work Plan

The study's work plan is developed to create a visual reference for workflow management and milestone achievement, as shown in Figure 3.8.

No.	Project Activities	Planned Completion Date	W1	W2	W3	W4	W5	W6	W7	W8	W9	W10	W11	W12	W13	W14
Trimester 1																
1	Discuss the project details	6/17/2022														
2	Formulate general project overview	6/24/2022														
3	Identify the problem statement and important of study	7/8/2022														
4	Study the shading effect and sky models	8/19/2022														
5	Find literature, review and compile relevant studies into the report.	8/19/2022														
6	Record the preliminary results and report writing	9/2/2022														
7	Project Presentation	9/16/2022														
Trimester 2																
1	Study the temperature effect	3/11/2023														
2	Comparison of result between the Solargis data with the ground-based measurement	4/1/2023														
3	Documentation for the coding	4/8/2023														
4	Report writing: Revise introduction, literature review, methodology and analysis of result and discussion	4/22/2023														

Figure 3.8: Gantt Chart for the Project

3.9 Summary

The optimal tilt angle and orientation for different irradiance data and sky models will be determined using the pvlib library in Python programming. The shading factor is included to investigate the effect of partial shading on the optimal positioning of the PV system. The temperature effect is studied and analysed in the second phase.

CHAPTER 4

RESULTS AND DISCUSSION

4.1 Introduction

This chapter will study and analyse various relationships between optimal PV positioning, shading factor, and temperature effect, as shown in Figure 4.1. Different input horizontal irradiance data were utilised to study the impact of shading and temperature on PV performance.

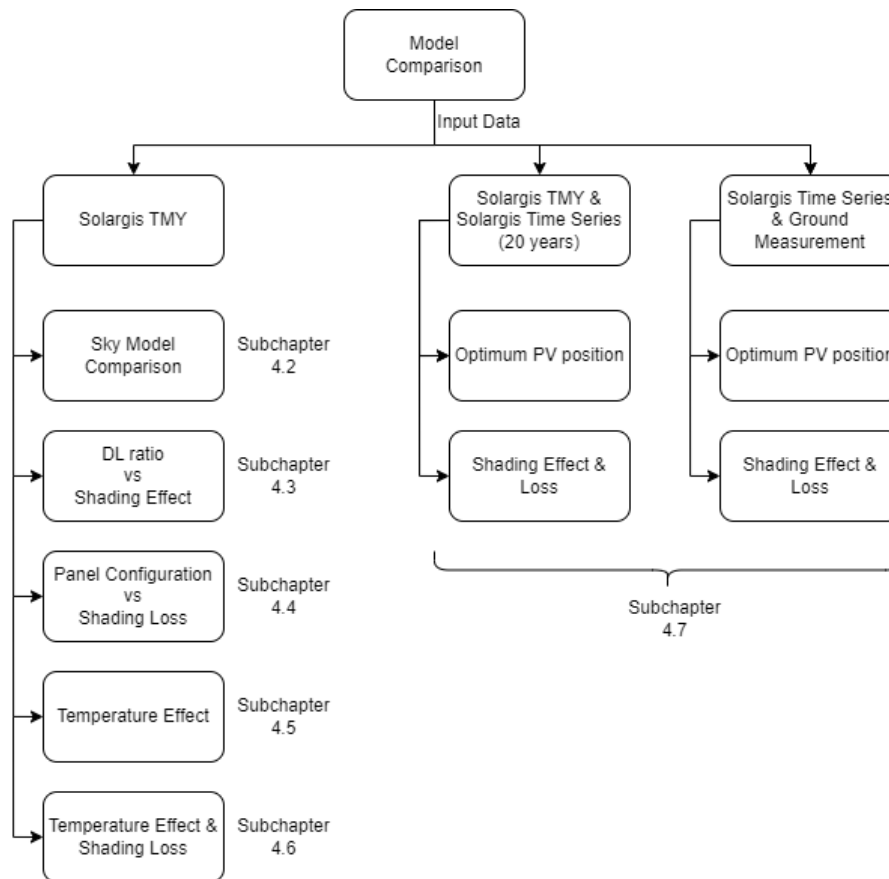


Figure 4.1: Analysis and Discussion Scope

4.2 Comparison between the Empirical Models

To study the different isotropic and anisotropic sky models employed to estimate the global tilted insolation, the meteorological data used was Solargis TMY by considering the inter-row shading effect with a DL ratio of 1.2. Figure 4.2 illustrates three polar contour plots; each represented the sky models used in the study. As can be observed, using the Perez model, the surface tilted with 6° , oriented slightly South of due East would harvest the maximum solar insolation of $1703.11 \text{ kWhm}^{-2}$ annually. The maximum annual global tilted irradiation (GTI) yielded were having slight differences for different empirical relations. The contour plots of percentage differences show the deviations between the sky models, as illustrated in Figure 4.3. The differences between the sky model are due to various parameters affecting the diffuse irradiance on the tilted surface. As for the Liu and Jordan model, the diffuse irradiance on an inclined plane depends only on the tilting angle. On the other hand, both Hay and Davies and Perez models consider the solar position, the angle of incidence, sky brightening, etc. Figure 4.4 displays the polar contour plots for the annual diffuse irradiation on the tilted surface based on the three types of transposition models.

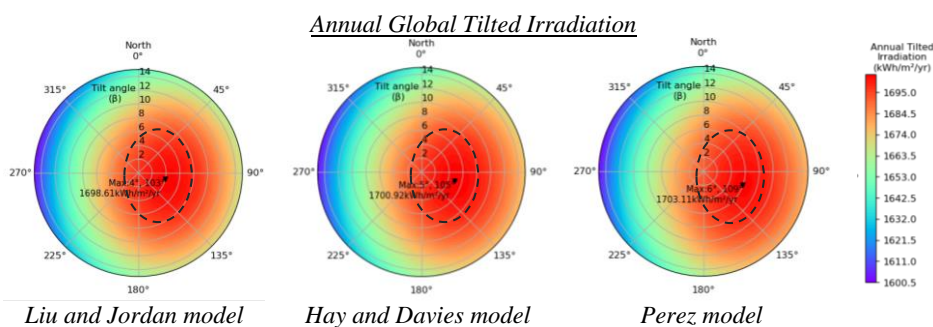


Figure 4.2: Annual GTI for Different Sky Models

Percentage Difference of Diffuse Component with respect to Perez Model

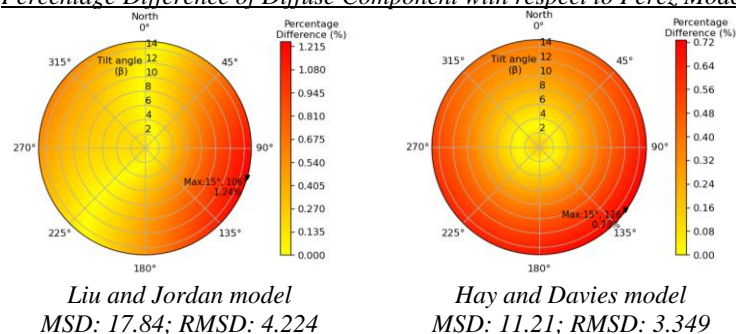


Figure 4.3: Percentage Difference between Sky Models

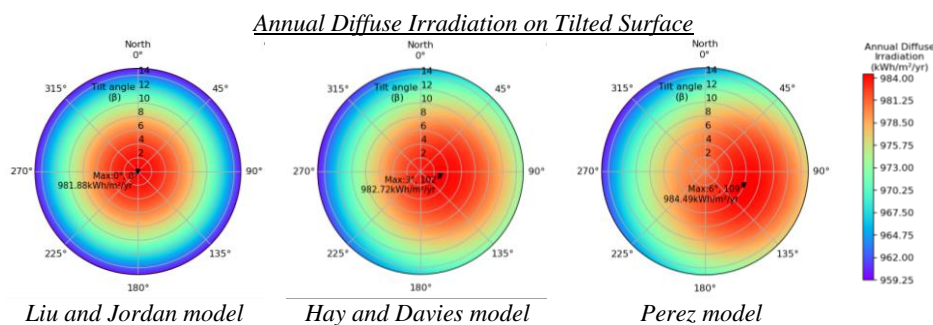


Figure 4.4: Annual Diffuse Irradiation on the Titled Surface for Different Sky Models

Nevertheless, the biggest percentage differences with reference to Perez model only happened at the large tilting angle of the PV module, which was only 1.24 % and 0.73 % for Liu and Jordan and Hay and Davies models, respectively. In addition, the RMSD of the Liu and Jordan model with respect to Perez model was about 4.224 kWhm^{-2} , whilst as for Hay and Davies model, the RMSD was slightly smaller, about 3.349 kWhm^{-2} . Within the high GTI region (circled with dotted lines), the percentage difference of GTI between Liu and Jordan and Perez models was below 0.5 %, while Hay and Davies model was about 0.4 %. This matches with the finding by Pandey and Katiyar (2009) and Shukla et al. (2015), whereby the isotropic and anisotropic models provide similar results for small PV tilt angles. As the tilt angle increases, the differences become more significant. It is because the module surface is almost parallel to the sky plane when the tilt angle is small. As a result, the distribution of the solar radiation on the module surface is relatively uniform, and the differences between isotropic and anisotropic models are minimum. As the tilt angle increases, the directional dependence of solar radiation in the anisotropic model becomes more significant and thus results in greater differences between the sky models.

4.3 Relationship between Different DL Ratios and Shading Effect

In this subchapter, the linear shading loss is considered by neglecting the bypass diode effect. Based on the input horizontal irradiance data from Solargis TMY, 11 contour plots were created to represent the annual global tilted irradiation at all possible tilt and azimuth angles with different DL ratios using the Perez model. All the plots shared the same legend, as shown in Figure 4.5. Generally, the pitch-distance-to-PV-length ratio (DL ratio) will influence the inter-row shading effect. At a DL ratio of 1.0, relatively high global tilted irradiation can be achieved at a low tilt angle. However, as the tilt angle rises, the shading effect due to the PV front row becomes more noticeable, reducing the amount of solar irradiance the PV module receives. When the DL ratio increases beyond 1.2, the shading effect becomes less significant, allowing higher tilt angles to be used to maximise the amount of in-plane solar irradiance. As a result, the polar contour plots after a DL ratio of 1.2 looks similar to each other.

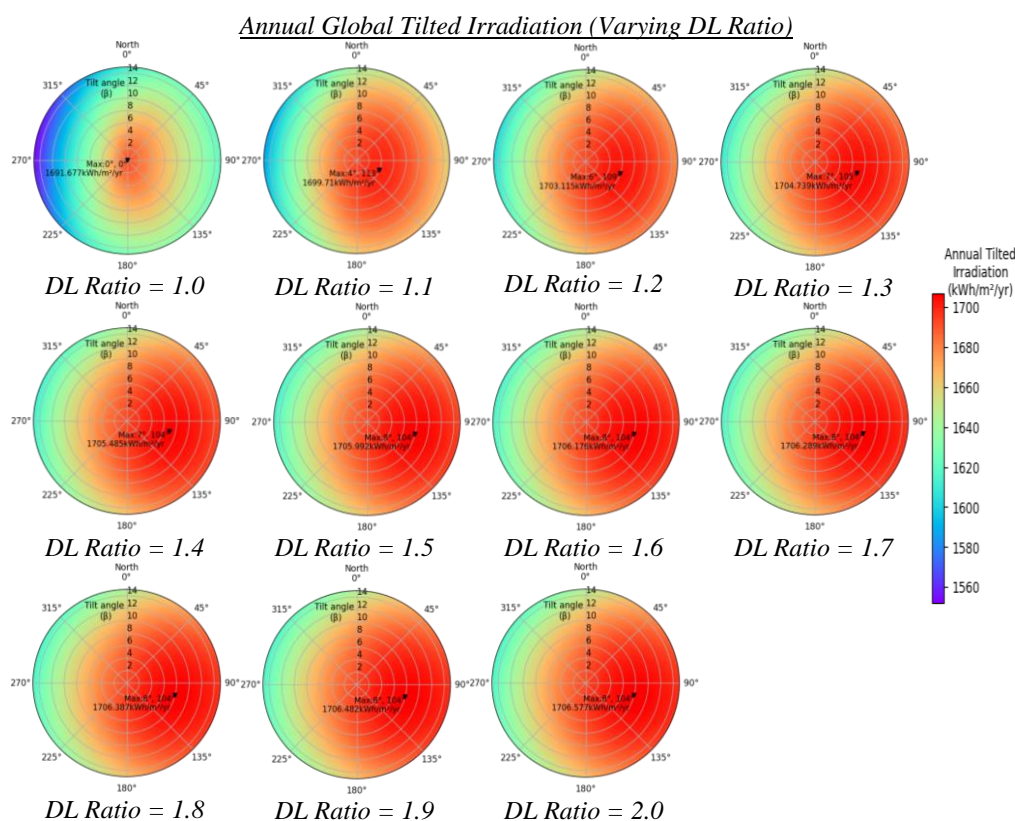


Figure 4.5: Annual GTI for Different DL Ratios.

Quantifying the inter-row shading loss is one of the essential factors to consider in optimizing the performance of PV systems. In this study, the amount of inter-row shading loss was quantified by comparing the results obtained from considering and not considering shading. This comparison was based on the calculation of different statistical metrics such as MAD, RMSD, MAPD and HAPD. The differences between the shading for different DL ratios and non-shading were computed for all possible orientation and tilting angles. The average of the differences for all angles was calculated in the case of MAD, MAPD and RMSD. These metrics can provide a comprehensive understanding of the magnitude and nature of shading loss in the unit of kWh/m² and %. As observed from Figure 4.6, the annual shading loss decreases exponentially as the DL ratio increases. At a DL ratio of 1.0, the highest annual shading loss is recorded, about 36 kWh/m² and 4.59 %, in terms of RMSD and HAPD, respectively. Once the DL ratio is beyond 1.3, the shading loss caused by front-row PV becomes less than 1 % or 5 kWh/m² annually.

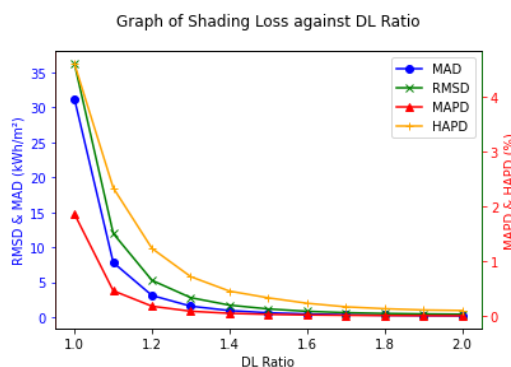


Figure 4.6: Effect of DL Ratio on the Inter-row Shading Loss

Figure 4.7 illustrates the impact of varying the DL ratio on the maximum GTI yielded, optimal tilt, and surface azimuth angles. The results show that the optimal surface azimuth is almost independent of the DL ratio, with values ranging from 104 ° to 113 °. This indicates that the azimuth angle selection slightly South of due East can be less sensitive to the inter-row shading effects, giving a good suggestion for installing a PV system design. At a DL ratio of 1.0, since the optimal tilting angle is zero, the optimal surface azimuth angle can be in any direction.

Besides that, the effect of the DL ratio on the optimal tilt angle is found to be substantial. A large DL ratio will allow for a higher tilting angle, resulting

in a rise in the optimal tilt angle. Nevertheless, due to the reduction of shading loss at a greater DL ratio, the optimal tilt angle will tend to saturate at 8° after a DL ratio of 1.5. A similar behaviour can be seen in the effect of the DL ratio on the maximum annual GTI yielded by the PV system. Upon exceeding the DL ratio of 1.2, any increment in the DL ratio will not significantly improve the maximum annual GTI.

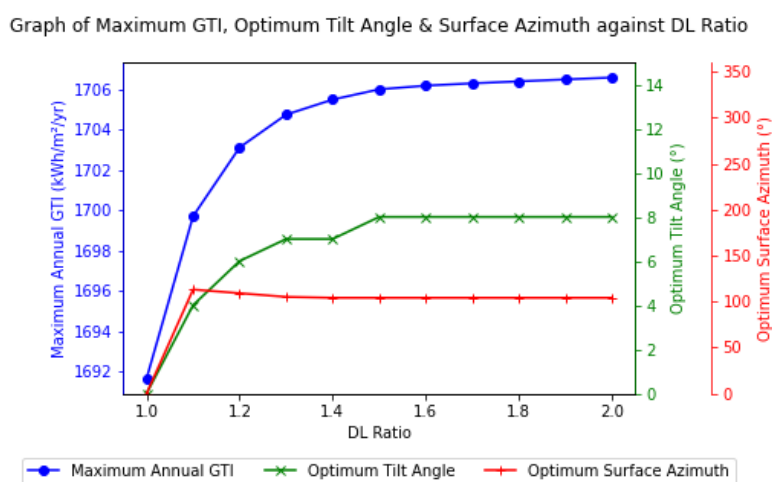


Figure 4.7: Effect of DL Ratio on the Maximum Annual GTI, PV Optimal Tilt and Surface Azimuth Angles

4.4 Comparison between Different PV Orientation Configurations

Sub-chapter 4.2 emphasizes that the inter-row shading effect is particularly significant when the DL ratio is below 1.2. In the current subchapter, a DL ratio of 1.1 was employed to explore the impact of various panel configurations on the PV shading loss. The results were generated using the Perez model and Solargis TMY horizontal solar irradiance data and compared to the shading effect that occurs when the bypass diode is not considered. In fact, the partial shading on the PV module can result in increased shading loss due to the bypass diode, making it crucial to determine the degree of power loss. The PV output power is directly related to the in-plane solar irradiance, making it possible to represent the net PV output power using the reduced equivalent solar irradiance due to the shading-bypass diode (RESIS) by neglecting other types of PV system losses.

Figure 4.8 and Figure 4.10 display the polar contour plots of RESIS for various panel configurations in landscape and portrait, respectively. When stacking the PV panels layer by layer in landscape orientation, the shading loss will be more similar to the partial shading without considering the bypass diode, as shown in Figure 4.8. This trend can be well explained using the graphs of shading loss against partial shading for different landscape configurations, as illustrated in Figure 4.9. As seen in Figure 4.9, in a 1-stacked landscape PV configuration, the shading loss occurs in three-step increments, with values of either 0, 0.33, 0.67, or 1. This means that any gradual shading on the PV module will ultimately result in higher loss. Hence, the RESIS polar contour plots of the 1-stacked landscape PV system reveal that a low tilt angle can yield high irradiation. However, the irradiation is greatly reduced at a high tilt angle facing due East or West. This is due to the long shadow casting on the adjacent PV row caused by a high tilt angle, leading to more significant shading loss. When more landscape-oriented PV modules are stacked, the graph approaches a close-to-linear shape with small increments. As a result, the RESIS contour plot of the 4-stacked landscape configuration is approximately identical to that of partial shading.

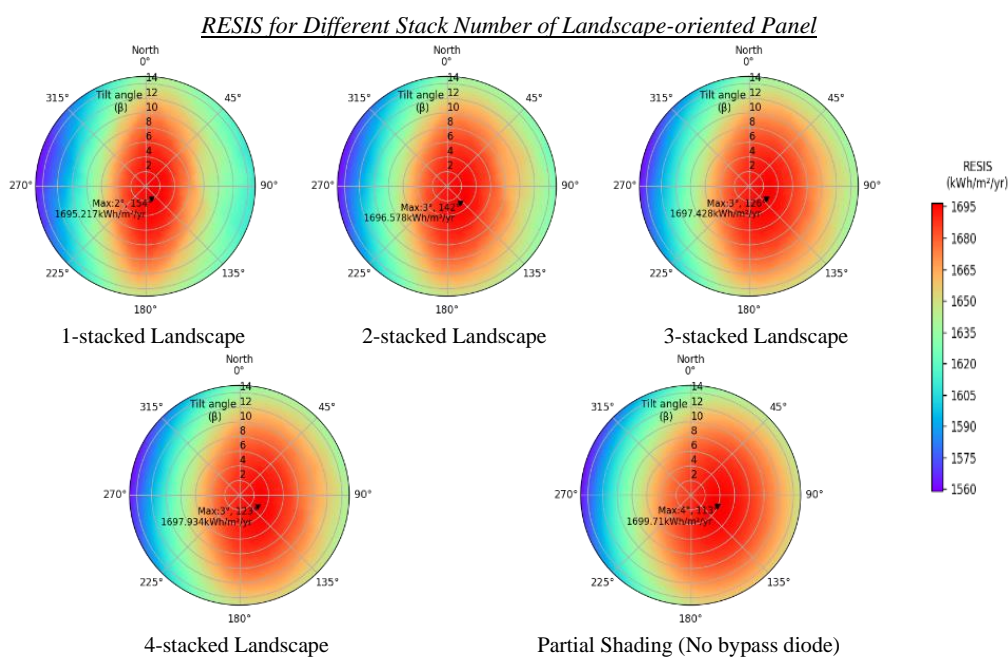


Figure 4.8: RESIS Polar Contour Plots for Different Stack Numbers of Landscape-oriented Panel

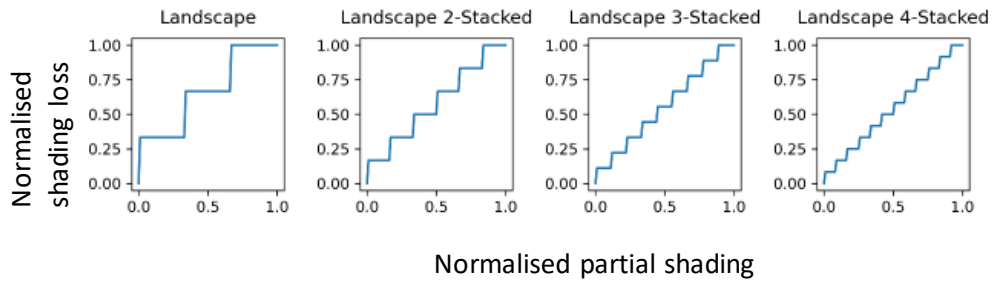


Figure 4.9: Graphs of Shading Loss against Partial Shading for Landscape-oriented PV

Furthermore, in the case of portrait-oriented PV systems, the partial shading can result in a total shading loss (normalised shading loss equals to 1.0) for a single stacked configuration. When two stacked configurations are used, the shading loss is slightly improved, providing an additional 50 % step increment, as shown in Figure 4.11. Nevertheless, the RESIS polar contour plots of portrait-oriented PV systems (Figure 4.10) show that the PV systems cannot accommodate high tilting angles when the DL ratio is 1.1.

RESIS for Different Stack Number of Portrait-oriented Panel

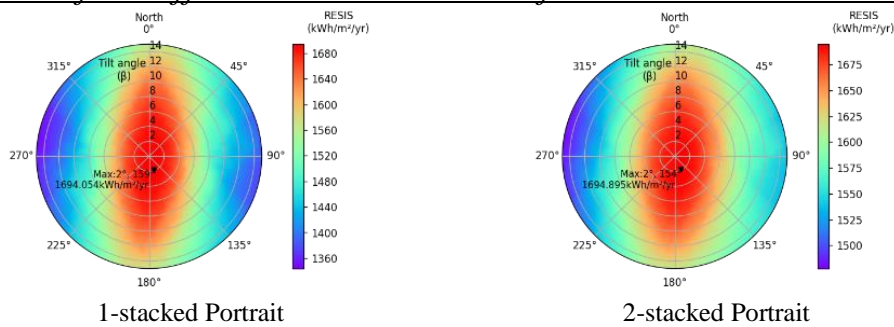


Figure 4.10: RESIS Polar Contour Plots for Different Stack Number of Portrait-oriented Panel

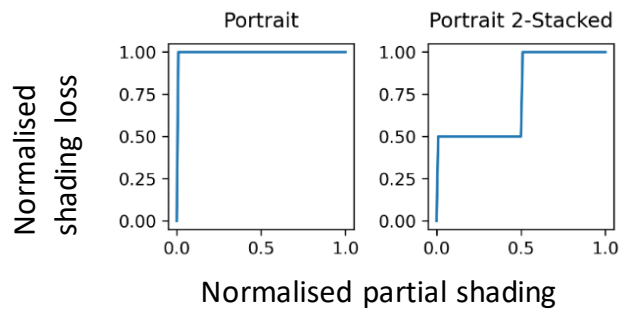


Figure 4.11: Graphs of Shading Loss against Partial Shading for Portrait-oriented PV

To quantify the shading loss due to bypass diodes for different panel configurations, the results were compared with and without the bypass diode by computing the four statistical metrics: RMSD and MAD in kWh/m², MAPD and HAPD in %, at DL ratio of 1.1. The shading loss finding for different panel configurations is summarized in Figure 4.12. Among the different panel configurations, the portrait 1-stacked (PT) configuration experienced the highest loss of 125.24 kWh/m² and 93.07 kWh/m², regarding RMSD and MAD, respectively, and 5.61 % and 16.27 %, for MAPD and HAPD, respectively. On the other hand, the configuration with the least shading loss was the landscape 4-stacked (LS 4-S) configuration, with 6.65 kWh/m² and 5.01 kWh/m², in terms of RMSD and MAD, respectively, and 0.3 % and 0.95 %, for MAPD and HAPD, respectively.

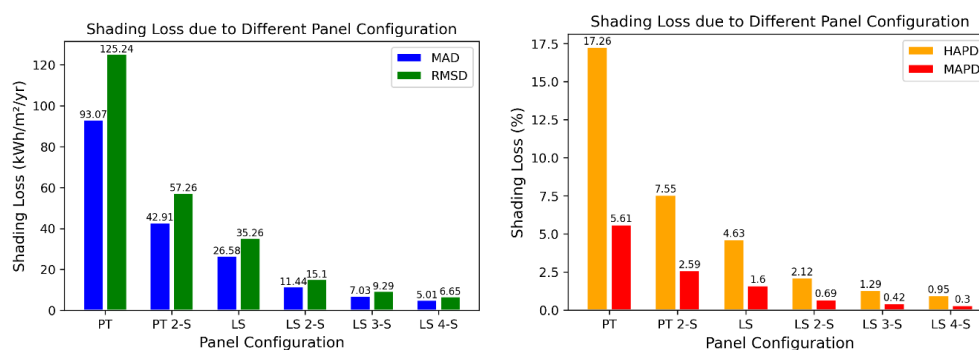


Figure 4.12: Shading Loss due to Bypass Diode for Different Panel Configuration. Note: The Abbreviation Meaning: PT: Portrait 1-stacked; PT 2-S: Portrait 2-stacked; LS: Landscape 1-stacked; LS 2-S: Landscape 2-stacked; LS 3-S: Landscape 3-stacked; and LS 4-S: Landscape 4-stacked.

The study also examined the effect of DL ratios on shading loss for various panel configurations. As shown in Figure 4.13, the shading loss decreases exponentially for different panel configurations as the DL ratio increases. The decreasing trend is due to the reduction in the inter-row shading effect as the distance between PV rows rises. When the DL ratio reaches and exceeds 1.4, the shading loss for all panel configurations reaches its minimum, which is less than 10 kWh/m² for MAD and RMSD, less than 1 % for MAPD,

and 3 % for HAPD. This indicates that for a DL ratio greater than 1.4, any panel configuration can achieve the minimum shading loss.

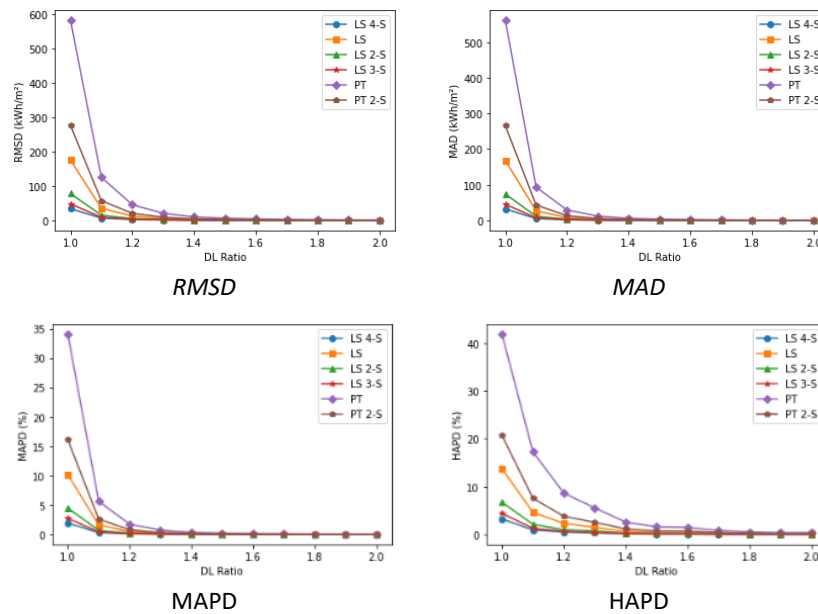


Figure 4.13: Shading Loss due to Bypass Diode for Different Panel Configurations and DL Ratios

In addition, the effect of the panel configuration on the optimal PV positioning was investigated in this study. The optimal tilt angle increases with the DL ratio, as shown in Figure 4.14 (a). For portrait (PT), portrait 2-stacked (PT 2-S), and landscape configurations, the optimal tilt angle is relatively smaller at a small DL ratio to reduce the inter-row shading effect. The optimal tilt angle for all panel configurations will saturate at 8° after a DL ratio of 1.6. As for the optimal surface azimuth, the PV azimuth angle is slightly East of due South for landscape, landscape 2-stacked, portrait, and portrait 2-stacked at a small DL ratio because of the south-facing experiencing the least shading. However, as the DL ratio increases, the optimal surface azimuth is facing slightly South of due East, around 104° , for all panel configurations, as shown in Figure 4.14 (b).

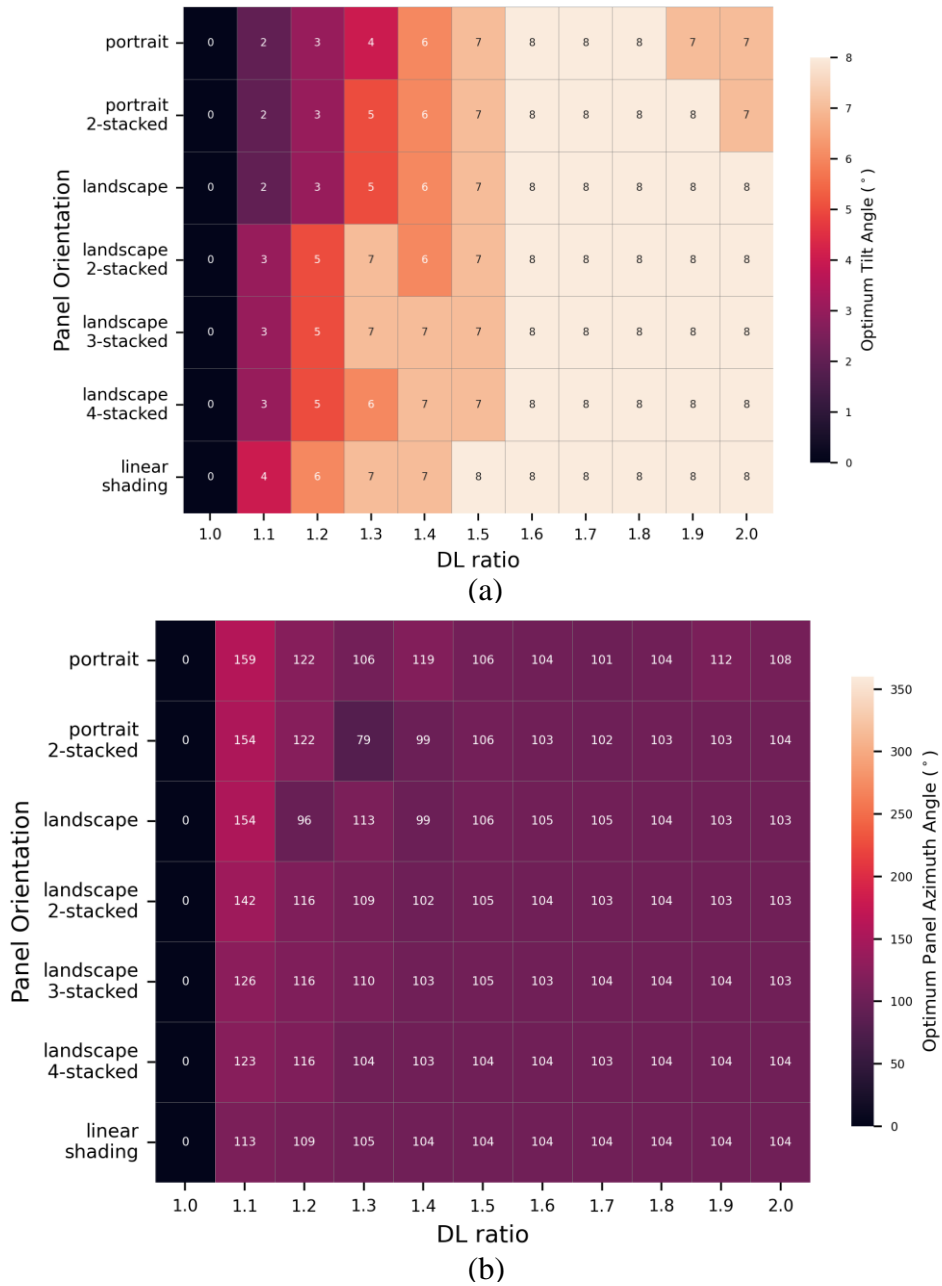


Figure 4.14: (a) Optimal Tilt Angle and (b) Surface Azimuth Angle for Different Panel Configurations and DL Ratio

4.5 Temperature Effect

The effect of module operating temperature on PV performance is studied using the Reduced Equivalent Solar Irradiation due to Temperature (RESIT), which represents the PV output power assuming an ideal system with no other losses. The PV module operating temperature is estimated using the Ross coefficient model and multiplied by the temperature coefficient to obtain the temperature factor. The temperature factor is then multiplied by the in-plane solar irradiance to obtain RESIT. Figure 4.15 shows the RESIT polar contour plots at two extreme DL ratio values, compared with the annual GTI plots considering the linear shading effect (no bypass diode). The contour plots exhibit similar trends for both cases at different DL ratios, but the overall magnitude of the irradiation decreases significantly after considering the temperature effect.

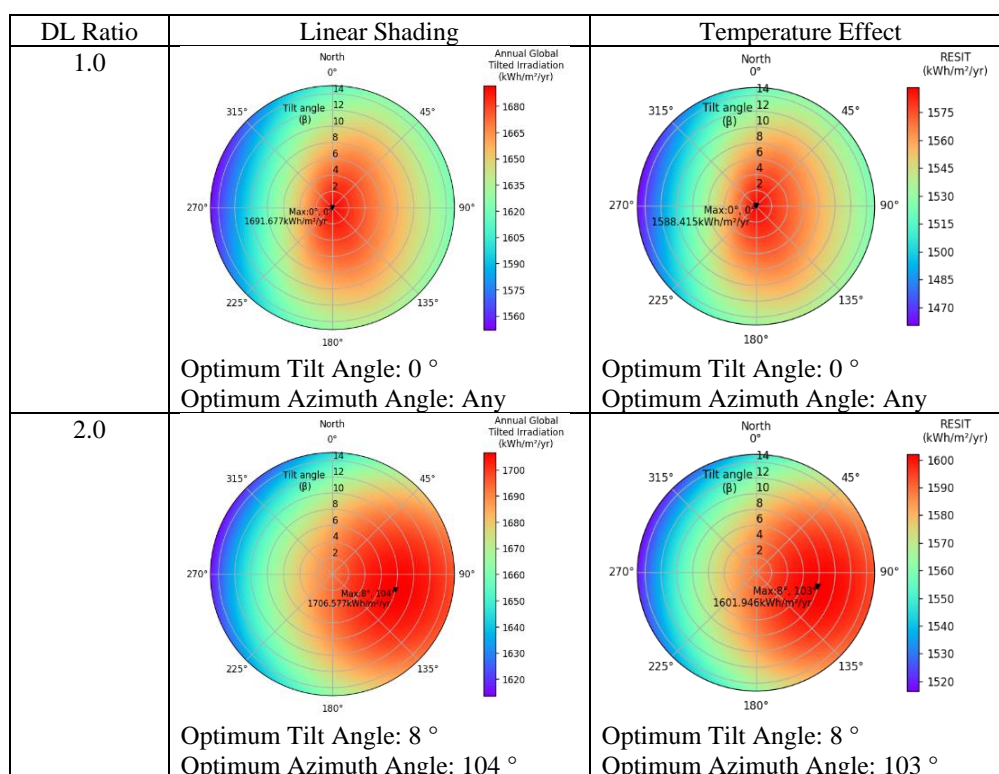


Figure 4.15: Comparison between RESIT and GTI Contour Plots

Since the overall trend of the solar irradiation distribution is not expected to change extensively, the PV optimal tilt angle and surface azimuth angle determined based on the maximum RESIT yielded will remain almost unchanged, as shown in Figure 4.16.

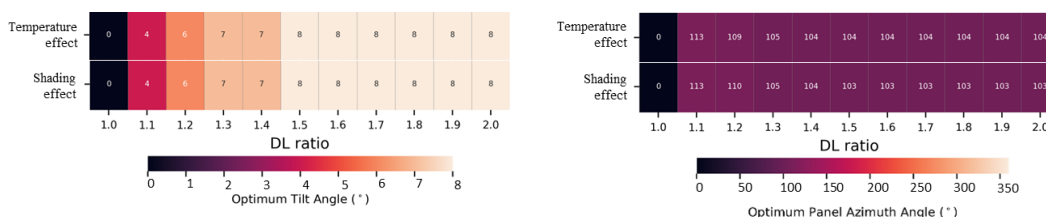


Figure 4.16: Optimal Tilt Angle and Surface Azimuth Angle Considering Temperature Effect

The drop in reduced equivalent solar irradiation (RESI) due to the temperature effect is determined by comparing the results with and without considering the temperature effect (which also refers to the difference between RESIS and RESIT). When the DL ratio is 1.0, the RESI decreases by about 99.5 kWh/m² and around 6 % due to the rise in the module temperature, as shown in Figure 4.17. As the DL ratio increases, the drop in the RESI becomes larger and reaches a saturation point of approximately 102.4 kWh/m² and 6.1 % after a DL ratio of 1.3. The great drop in RESI due to the temperature effect during a small DL ratio increment is due to a decline in the inter-row shading effect, resulting in a higher in-plane solar irradiance and module temperature. In addition, the saturation point suggests that the inter-row shading effect is minimal after a DL ratio of 1.3, with a constant in-plane solar irradiance and PV performance loss due to the temperature effect despite increasing the DL ratio.

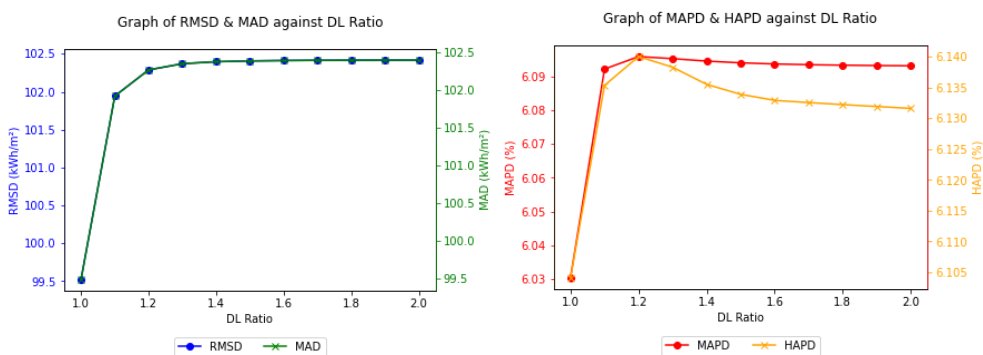


Figure 4.17: Effect of DL ratio on the drop in RESI due to temperature effect.

4.6 Temperature Effect and Shading Effect with Bypass Diode

This subchapter investigated the effect of DL ratio on the total drop in RESI due to temperature and shading effects caused by bypass diodes using different panel configurations. The analysis took into both factors and shows that the total drop in RESI is higher than that, as illustrated in Figure 4.13, as the temperature effect is considered. Figure 4.18 shows that the RESI drop will decrease as the DL ratio increases for all panel configurations. This is because the shading loss dominates the total drop in RESI, and increasing the DL ratio can eventually reduce it. Nonetheless, there is still a drop in RESI due to the temperature effect. After reaching saturation, the total drop in RESI is almost equivalent to the RESI drop due to the temperature effect.

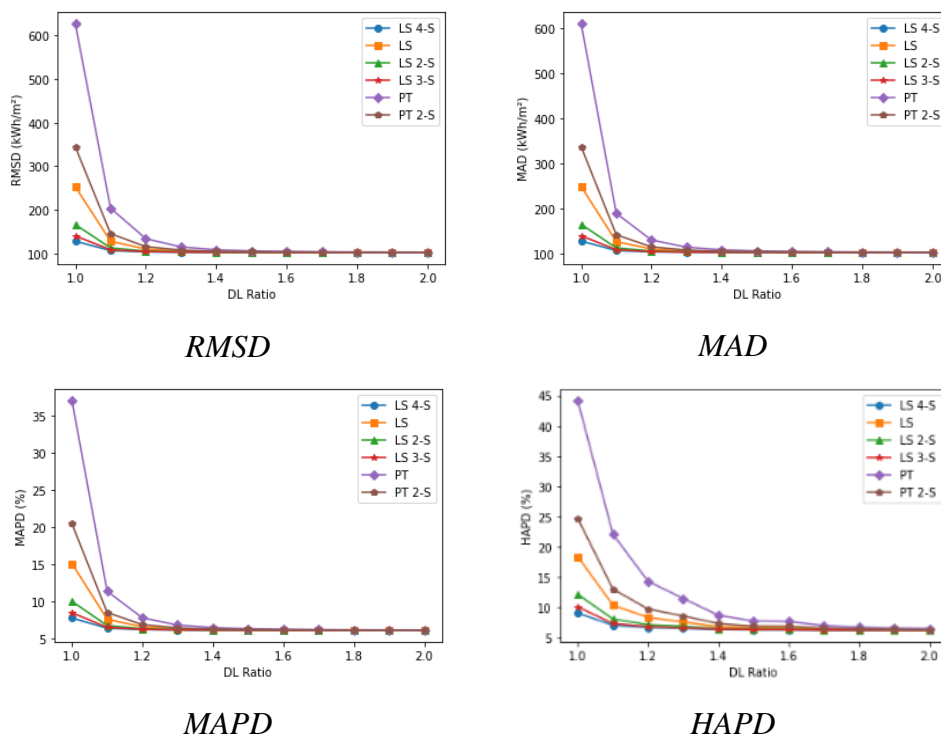


Figure 4.18: RESI Drop due to Temperature and Shading Effects with Bypass Diode for Different Panel Configurations and DL Ratios.

In subchapter 4.4, the results reveal that the temperature effect almost unaffected the optimal PV positioning. Therefore, the optimal tilt angle and surface azimuth angle considering both shading and temperature factors are approximately the same as those considering shading only. Figure 4.19 clearly

depicts the optimal PV installation angles for different panel configurations and DL ratios while considering both shading and temperature effect.

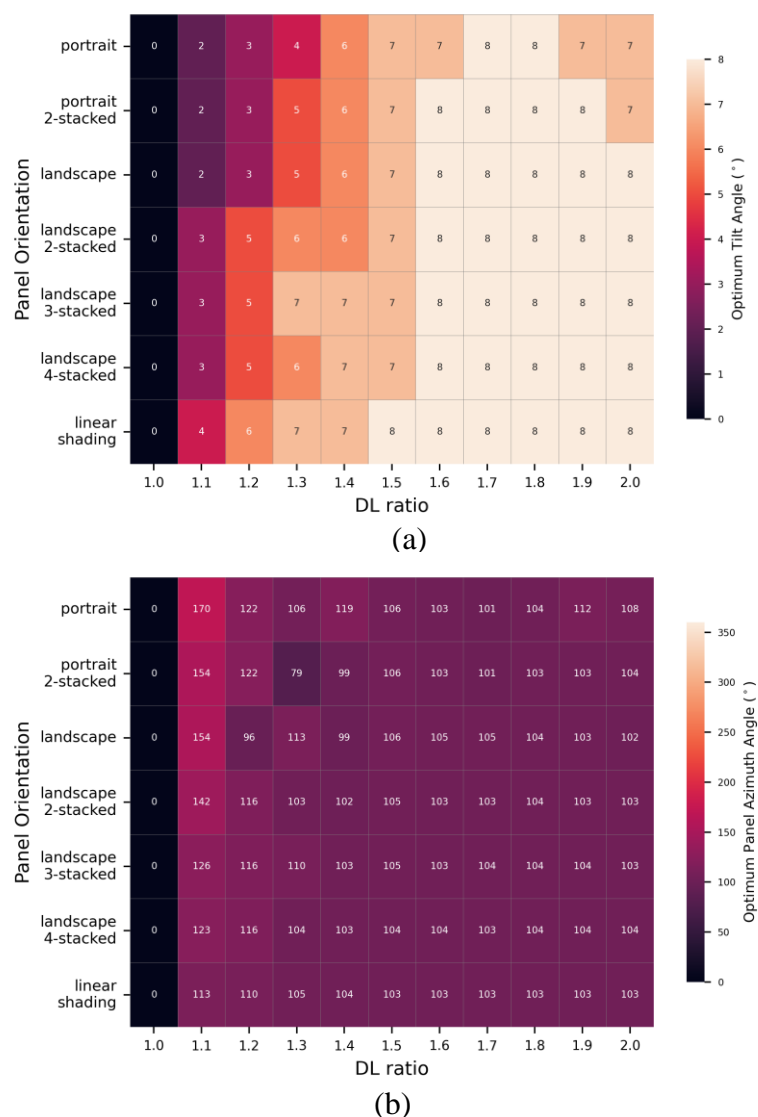


Figure 4.19: (a) Optimal Tilt Angle and (b) Surface Azimuth Angle for Different Panel Configurations and DL Ratio Considering Temperature and Shading Effects.

4.7 Study on the Input Solar Irradiance Data and Optimal PV Positioning

This study investigated the effect of sky models on the optimal tilt angle and the surface azimuth of solar panels, considering the shading effect only and using the Solargis TMY data. Three sky transposition models, namely Liu and Jordan, Hay and Davies, and Perez model, were utilized in the investigation for various

panel configurations at different DL ratios. The temperature effect is not considered, as it merely affects the optimal PV positioning. The results reveal that the optimal tilt angle for the Perez model is slightly higher than that of the Hay and Davies model, while the Hay and Davies model is larger than the Liu and Jordan model, as shown in Figure 4.20. Regardless of the sky model used, the optimal surface azimuth faces approximately slightly South of due East direction. Table 4.1 illustrates the optimal tilting angles and orientations of deploying the three sky models at a DL ratio of 1.2. Furthermore, the maximum annual solar irradiation (or RESIS) exhibits a trend similar to the tilt angle, where the Perez model yields the highest values, followed by the Hay and Davies model and the Liu and Jordan model. These findings provide an overall picture of the impact of the sky models on the positioning of solar panels for optimal energy generation.

In addition, a comparison and evaluation of the accuracy of the Solargis TMY data, which represents the standardized weather data for a specific location and reflects a long-term weather pattern, was done. The Solargis time series data, which are the collected weather measurement taken at a fixed interval over time, were used to carry out this comparison. To conduct the comparison, 20 years of time series data (from 1st January 2002 to 31st December 2021) with an interval of 30 minutes are utilised, and the average global tilted irradiation (or RESIS) is computed using the steps outlined in Figure A-1. The results obtained from both the Solargis TMY and 20-year time series data showed almost the same trend, with a slight deviation in values, as illustrated in Figure 4.20. Furthermore, the optimal tilt and azimuth angles for both cases closely matched each other. These findings suggest that the Solargis TMY data can be used confidently to estimate a specific location's long-term solar energy potential with high accuracy.

This paper also compared the results generated based on ground-based solar irradiance measurements with the Solargis time series data for 2020 with a 30-minute interval using the Hay and Davies model. The Hay and Davies model is deployed because its estimation values fall between the Liu and Jordan and Perez models. Generally, the ground-based measurements are lower than the satellite-derived data (Solargis) due to various factors, such as local weather conditions, which can block or scatter the incoming solar radiation and reduce

the measured irradiance values. Therefore, from Figure 4.21, it can be seen that the maximum solar irradiation computed using ground-based measurement data is smaller than that of using Solargis time series data. Additionally, the optimal tilt angle estimated by using the ground-based measurement data is larger than that of using the Solargis data by 1 to 3°. The optimal surface azimuth also deviates slightly but generally still faces the direction slightly South of due East.

Last but not least, the effect of the input data resolution on the optimal PV installation angle was also investigated using the ground-based measurement with 1-hour and 30-minute intervals. The results depict some insignificant deviations in the optimal tilt angle, surface azimuth and maximum solar irradiation (or RESIS) for different panel configurations and DL ratio when different data resolutions are being used, as shown in Figure 4.21.

Table 4.2 summarises the lists of optimal tilting angles and orientations and maximum RESIS yielded based on different input horizontal solar irradiance data by utilising the Perez model with the landscape 2-stacked panel configuration and DL ratio of 1.4. This table clearly shows the effect of the data used on these three parameters, as discussed above.

Table 4.1: Optimal Tilting Angle and Orientation, and Maximum GTI Yielded for Different Sky Models at DL Ratio of 1.2.

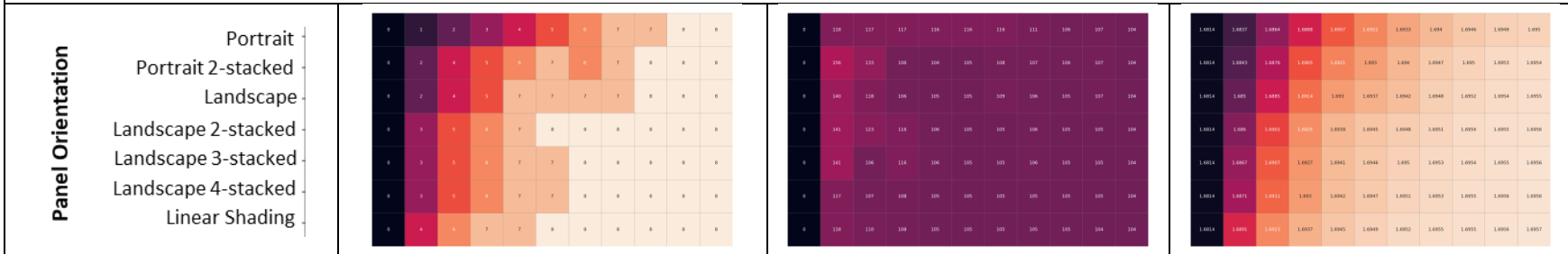
Sky Models	Optimal Tilting Angle (°)	Optimal Surface Azimuth (°)	Maximum GTI (kWh/m²)
Liu and Jordan	4	103	1698.61
Hay and Davies	5	105	1700.92
Perez	6	109	1703.11

Table 4.2: Summary Table for Optimal Tilting Angle and Orientation, and Maximum RESIS Yielded for Different Types of Horizontal Solar Irradiance Data using Perez Model with Landscape 2-stacked Configuration and DL Ratio of 1.4.

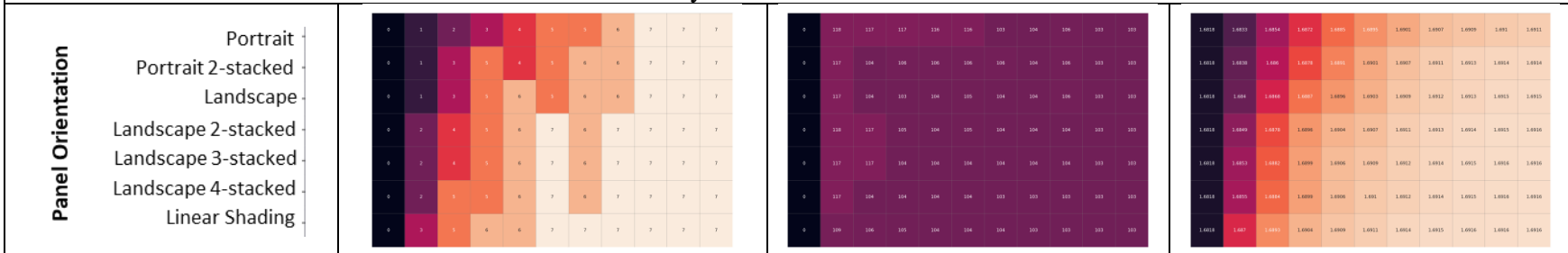
Type of Horizontal Solar Irradiance Data	Optimal Tilting Angle (°)	Optimal Surface Azimuth (°)	Maximum RESIS (kWh/m²)
Solargis TMY	6	102	1704.57
Solargis Time Series Data (30-min interval: 20 years)	7	106	1693.94
Solargis Time Series Data (30-min interval: 2020)	7	105	1687.64
Ground Measurement Data (30-min interval: 2020)	9	107	1597.71
Ground Measurement Data (1-hour interval: 2020)	9	107	1600.05

Horizontal Irradiance Data: Solargis Time Series Data with a 30-minute time step (from 1st January 2002 to 31st December 2021)

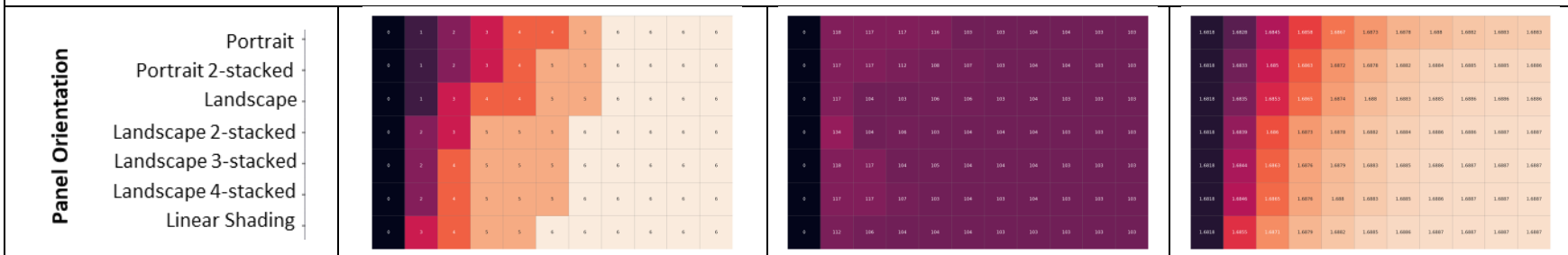
Perez model

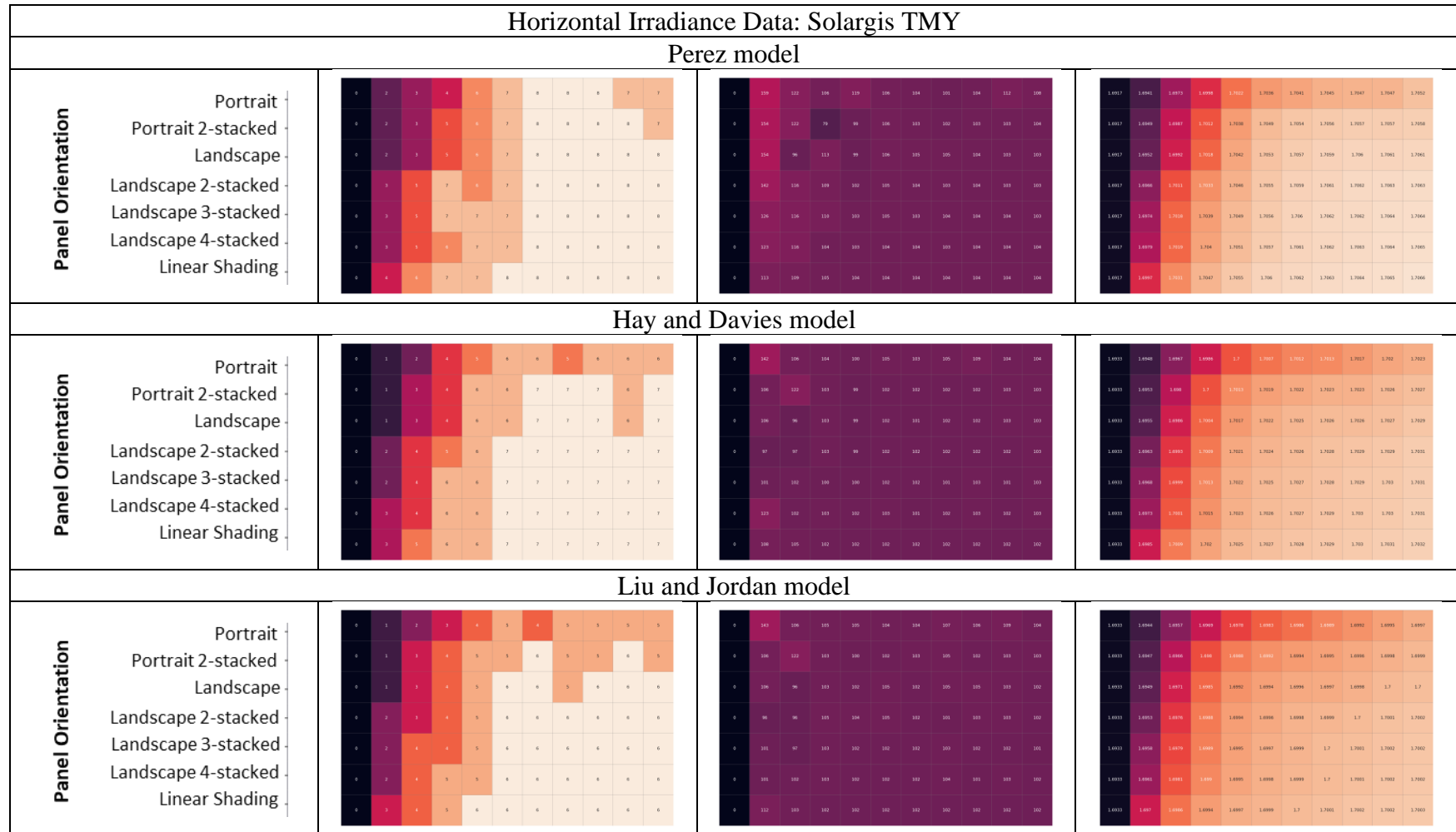


Hay and Davies model



Liu and Jordan model





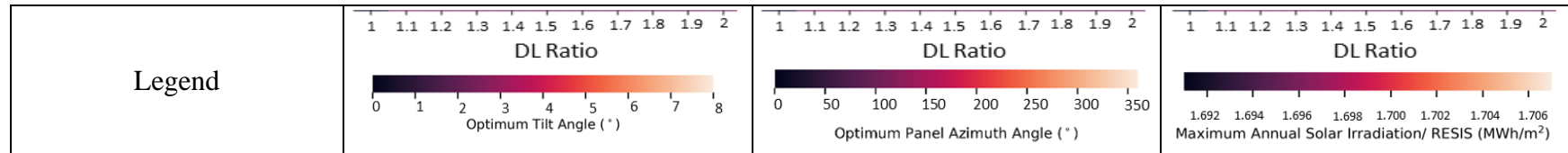
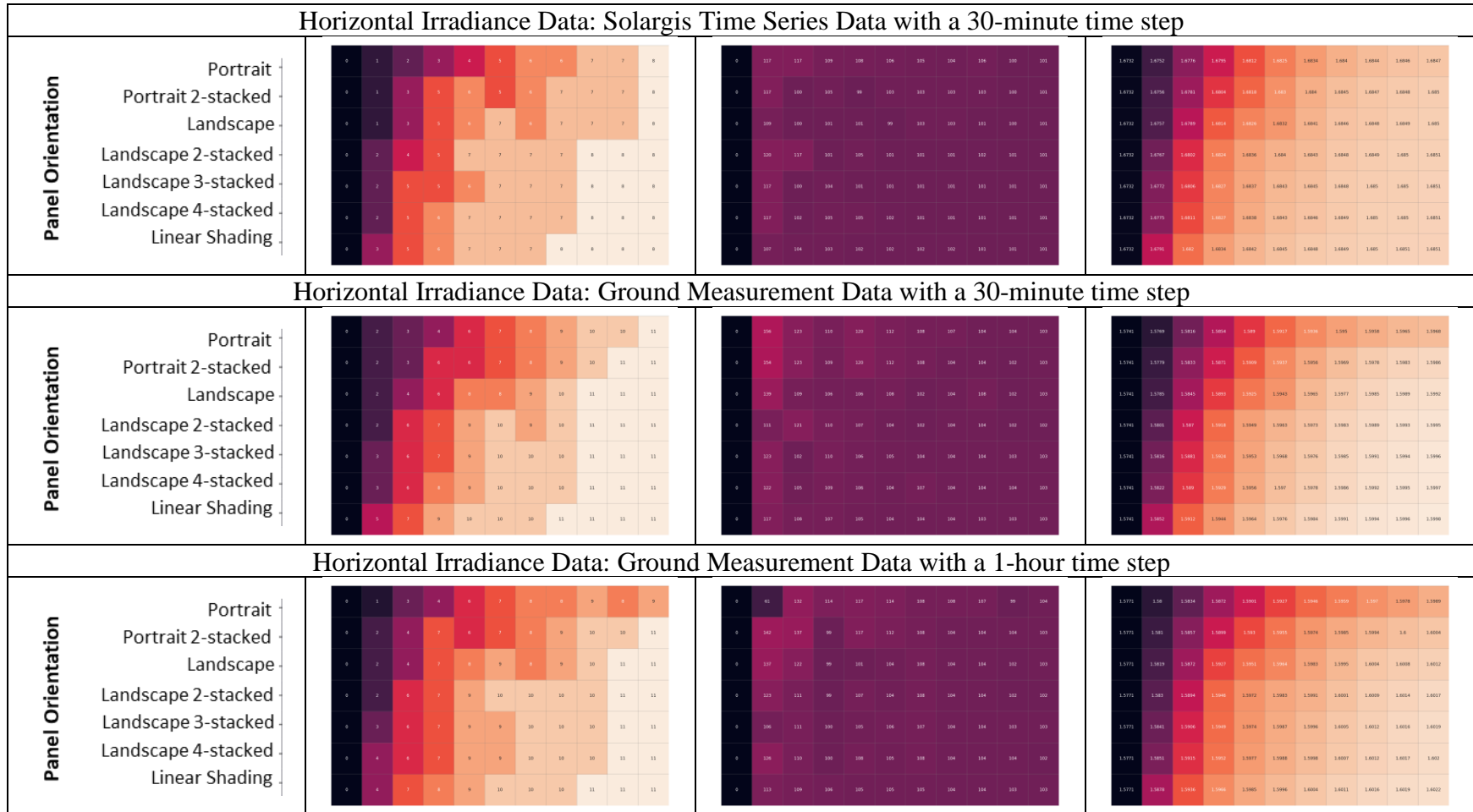


Figure 4.20: Optimal Tilt Angle, Surface Azimuth and Maximum Solar Irradiation (or RESIS) Estimated using Solargis TMY and 20-year Time Series Data.



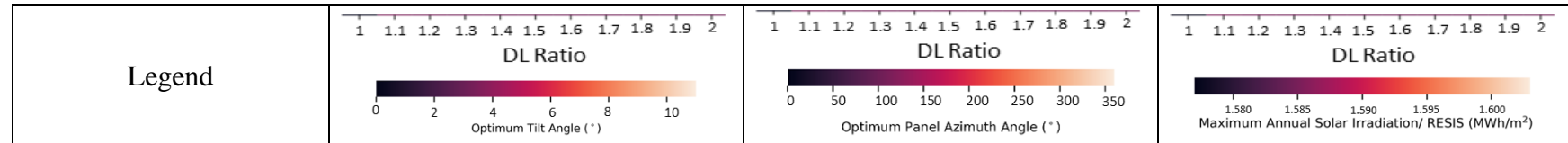


Figure 4.21: Optimal Tilt Angle, Surface Azimuth and Maximum Solar Irradiation (or RESIS) Estimated Based on Solargis Time Series Data and Ground-based Measurement Data Using Hay and Davies Model for Year 2020

4.8 Summary

This chapter investigated the effect of DL ratio on inter-row shading, the effect of panel configurations on shading loss, the effect of module temperature on PV output power, and the combined effects of temperature and shading. Different input horizontal solar irradiance data were utilised, and result comparisons were made among them.

CHAPTER 5

CONCLUSIONS AND RECOMMENDATIONS

5.1 Conclusions

The objectives of the study are achieved. This study investigated the impacts of transposition sky models, inter-row shading effect, bypass diode effect for different panel configurations, and module operating temperature on the optimal PV positioning. Based on the comparison among the three types of sky models (Liu and Jordan, Hay and Davies, and Perez models), the differences in the annual diffuse irradiation on tilted surfaces are less than 2 % for module tilting angles below 15 °. The Perez model and Solargis TMY solar irradiance database are utilized to examine the shading and temperature effects. The optimal tilting angle simulated using Perez model is found to be larger than that of the Hay and Davies model by 1 °, and the latter suggests a tilt of 1 ° higher than that of the Liu and Jordan model. In addition, the linear shading losses decrease exponentially as the DL ratio increases and saturate once the DL ratio is beyond 1.3, indicating that the shading effect is no longer significant. The optimal tilting angle rises substantially with the DL ratio, ranging from 0 ° to the saturation point of 8 ° after the DL ratio of 1.5, while the optimal surface azimuth is found to be slightly South of due East (ranging from 104 ° to 113 °), considering linear shading. With the bypass diode, the shading loss may be higher depending on the panel configurations. The RESIS yielded for the landscape 4-stacked configuration is the highest and closer to the annual GTI value considering linear shading (no bypass diode). In contrast, the portrait 1-stacked configuration yielded the least RESIS. When the DL ratio is small (less than 1.1), the optimal orientations for landscape 1- and 2-stacked and portrait 1- and 2-stacked configurations are facing the direction slightly East of due South (ranging from 142 ° to 159 °). For other panel configurations or beyond the DL ratio of 1.1, the optimal orientations will face slightly South of due East. The optimal tilt angle for all panel configurations will saturate at 8 ° after a DL ratio of 1.6. Besides that, the RESIT yielded by the PV module is lower than the RESIS because the module operating temperature significantly reduces the PV

output power. Nevertheless, the temperature effect merely affects the optimal PV positioning.

The differences in the optimal PV positioning are trivial when Solargis TMY and 20-year Solargis Time Series data are used. On the other hand, the optimal tilting angle estimated by ground-based measurement data is larger than that of using Solargis Time Series data by 1 to 3°. The optimal orientations remain consistent for all types of input data, barely deviating from the trend discussed above.

In short, the optimal tilting angle of the PV array depends on the DL ratio and panel configuration after considering the shading effect. The optimal surface azimuth angle is facing the direction of slightly South of due East (104°-122°). The temperature effect does not significantly impact the optimal PV positioning but decreases the RESIT yielded in all directions. The suggested DL ratio is about 1.3 with the landscape 4-stacked configuration to minimize the shading effect and loss. With the result found, this study hopes to give the industry a guideline to install at optimal orientation and tilting angles to yield the maximum output of PV by considering the losses due to shading and temperature.

5.2 Recommendations for future work

Solar energy has emerged as a promising solution for sustainable and renewable energy sources to address world climate change and reduce carbon emissions. A comprehensive understanding of the PV behaviour under various environmental conditions is necessary to fully realise the PV potential. Several future works are suggested to improve this study in optimizing the design and deployment of the PV systems:

- Extending the project study conducted at UTAR Sg Long, Kajang to other locations in Malaysia is recommended to gain a better insight into the PV system performance in different climates.
- To improve the accuracy of the shading factor calculation, it is suggested to use a 3D vector approach instead of the 2D trigonometric approach that assumes infinite row length.

- The conventional Ross model can be replaced with the time-specific Ross coefficient model developed by Lai and Lim (2019) to obtain more accurate module temperature predictions.
- Investigating other mounting types and PV cell technologies can provide valuable insights into PV system performance under different conditions.

REFERENCES

- Abdullahi, B. et al., 2020. Optimal Tilt Angle for Solar Collectors used in Kano, Nigeria. *Journal of Advanced Research in Fluid Mechanics and Thermal Sciences*, 56(1), pp.31–42. Available at: <https://akademiabaru.com/submit/index.php/arfmts/article/view/2483>.
- Adeeb, J., Farhan, A. and Al-Salaymeh, A., 2019. Temperature Effect on Performance of Different Solar Cell Technologies. *Journal of Ecological Engineering*, 20(5), pp.249–254.
- Al-Quraan, A. et al., 2022. Minimizing the Utilized Area of PV Systems by Generating the Optimal Inter-Row Spacing Factor. *Sustainability*, 14(10), p.6077.
- Aoun, N., 2022. Methodology for predicting the PV module temperature based on actual and estimated weather data. *Energy Conversion and Management: X*, 14, p.100182.
- Appelbaum, J. and Bany, J., 1979. Shadow effect of adjacent solar collectors in large scale systems. *Solar Energy*, 23(6), pp.497–507.
- Barreiro, C., Jansson, P.M., Thompson, A. and Schmalzel, J.L., 2011. PV bypass diode performance in landscape and portrait modalities. *Conference Record of the IEEE Photovoltaic Specialists Conference*. 2011 pp. 003097–003102.
- Cascone, Y., Corrado, V. and Serra, V., 2011. Calculation procedure of the shading factor under complex boundary conditions. *Solar Energy*, 85(10), pp.2524–2539.
- Castellano, N.N., Gázquez Parra, J.A., Valls-Guirado, J. and Manzano-Agugliaro, F., 2015. Optimal displacement of photovoltaic array's rows using a novel shading model. *Applied Energy*, 144, pp.1–9.
- Deline, C., 2009. Partially shaded operation of a grid-tied PV system. *2009 34th IEEE Photovoltaic Specialists Conference (PVSC)*. June 2009 IEEE, pp. 001268–001273.
- Dubey, S., Sarvaiya, J.N. and Seshadri, B., 2013. Temperature Dependent Photovoltaic (PV) Efficiency and Its Effect on PV Production in the World – A Review. *Energy Procedia*, 33, pp.311–321.
- Duffie, J.A. and Beckman, W.A., 2013. *Solar Engineering of Thermal Processes*, John Wiley & Sons, Inc., Hoboken, NJ, USA.
- Elhassan, Z.A.M., Zain, Muhammad.Fauzi.M., Sopian, K. and Awadalla, A., 2011. Output Energy of Photovoltaic Module Directed at Optimal Slope Angle in Kuala Lumpur, Malaysia. *Research Journal of Applied Sciences*, 6(2), pp.104–109.

Elhub, B. et al., 2012. Optimizing tilt angles and orientations of solar panels for Kuala Lumpur, Malaysia. , 7, pp.3758–3765.

eppleylab.com, *Shade Disk Kit* [Online]. Available at: <http://www.eppleylab.com/instrument-list/shade-disk-kit/> [Accessed: 6 September 2022].

F. Holmgren, W., W. Hansen, C. and A. Mikofski, M., 2018. pvlib python: a python package for modeling solar energy systems. *Journal of Open Source Software*, 3(29), p.884.

Fadaeenejad, Mohsen et al., 2015. Optimization and comparison analysis for application of PV panels in three villages. *Energy Science & Engineering*, 3(2), pp.145–152.

Figgis, B. and Abdallah, A., 2019. Investigation of PV yield differences in a desert climate. *Solar Energy*, 194, pp.136–140.

Hailu and Fung, 2019. Optimal Tilt Angle and Orientation of Photovoltaic Thermal System for Application in Greater Toronto Area, Canada. *Sustainability*, 11(22), p.6443.

Handoko Rusiana, I., Yuda Bakti, Z. and Sambasri, S., 2018. Study and Analysis of Shading Effects on Photovoltaic Application System. *MATEC Web of Conferences*, 218, p.02004.

Hay, J.E. and Davies, J.A., 1980. Calculation of the solar radiation incident on an inclined surface. *Proceedings: First Canadian Solar Radiation Data Workshop*. 1980 Toronto, Ontario, Canada , pp. 59–72.

Jacobson, M.Z. and Jadhav, V., 2018. World estimates of PV optimal tilt angles and ratios of sunlight incident upon tilted and tracked PV panels relative to horizontal panels. *Solar Energy*, 169, pp.55–66.

Khatib, T., Mohamed, A., Mahmoud, M. and Sopian, K., 2015. Optimization of the Tilt Angle of Solar Panels for Malaysia. *Energy Sources, Part A: Recovery, Utilization, and Environmental Effects*, 37(6), pp.606–613.

Khoo, Y.S. et al., 2014. Optimal Orientation and Tilt Angle for Maximizing in-Plane Solar Irradiation for PV Applications in Singapore. *Photovoltaics, IEEE Journal of*, 4, pp.647–653.

Lai, K.-Y. and Lim, B.-H., 2019. Comparative Study for Time-specific Ross Coefficient and Overall Ross Coefficient for Estimation of Photovoltaic Module Temperature. *2019 IEEE Conference on Sustainable Utilization and Development in Engineering and Technologies (CSUDET)*. 2019 pp. 251–256.

Liu, B.L. and Jordan, R., 1961. Daily insolation on surfaces tilted towards equator. 1961

Loutzenhiser, P.G. et al., 2007. Empirical validation of models to compute solar irradiance on inclined surfaces for building energy simulation. *Solar Energy*, 81(2), pp.254–267.

Mamun, M.A.A. et al., 2017. Determining the optimal tilt angle and orientation for photovoltaic (PV) systems in Bangladesh. *2017 2nd International Conference on Electrical & Electronic Engineering (ICEEE)*. December 2017 IEEE, pp. 1–4.

Matius, M.E. et al., 2021. On the Optimal Tilt Angle and Orientation of an On-Site Solar Photovoltaic Energy Generation System for Sabah's Rural Electrification. *Sustainability*, 13(10), p.5730.

Melo, E.G., Almeida, M.P., Zilles, R. and Grimoni, J.A.B., 2013. Using a shading matrix to estimate the shading factor and the irradiation in a three-dimensional model of a receiving surface in an urban environment. *Solar Energy*, 92, pp.15–25.

Nordmann, T. and Clavadetscher, L., 2003. Understanding temperature effects on PV system performance. *3rd World Conference on Photovoltaic Energy Conversion, 2003. Proceedings of*. 2003 pp. 2243-2246 Vol.3.

Olukan, T.A. and Emziane, M., 2014. A Comparative Analysis of PV Module Temperature Models. *Energy Procedia*, 62, pp.694–703.

Oufettoul, H. et al., 2023. Comparative Performance Analysis of PV Module Positions in a Solar PV Array Under Partial Shading Conditions. *IEEE Access*, 11, pp.12176–12194.

Pandey, C.K. and Katiyar, A.K., 2009. A note on diffuse solar radiation on a tilted surface. *Energy*, 34(11), pp.1764–1769.

Pannebakker, B.B., de Waal, A.C. and van Sark, W.G.J.H.M., 2017. Photovoltaics in the shade: one bypass diode per solar cell revisited. *Progress in Photovoltaics: Research and Applications*, 25(10), pp.836–849.

Paudyal, B.R. and Imenes, A.G., 2021. Investigation of temperature coefficients of PV modules through field measured data. *Solar Energy*, 224, pp.425–439.

Perez, R. et al., 1990. Modeling daylight availability and irradiance components from direct and global irradiance. *Solar Energy*, 44(5), pp.271–289.

pvsyst.com, *Shading factor table* [Online]. Available at: https://www.pvsyst.com/help/shadings_factor_table.htm [Accessed: 6 September 2022].

Quaschnig, V. and Hanitsch, R., 1998. Increased Energy Yield of 50% at Flat Roof and Field Installations with Optimized Module Structures. *2nd World Conference and Exhibition on Photovoltaic Solar Energy Conversion*. 10 July 1998 Vienna, Austria.

Ross, R.G., 1976. Interface design considerations for terrestrial solar cell modules. 1976

Saint-Drenan, Y.-M. and Barbier, T., 2019. Data-analysis and modelling of the effect of inter-row shading on the power production of photovoltaic plants. *Solar Energy*, 184, pp.127–147.

seda.gov.my, *Renewable Energy in Malaysia* [Online]. Available at: <https://www.seda.gov.my/reportal/> [Accessed: 6 September 2022].

Shukla, K.N., Rangnekar, S. and Sudhakar, K., 2015. Comparative study of isotropic and anisotropic sky models to estimate solar radiation incident on tilted surface: A case study for Bhopal, India. *Energy Reports*, 1, pp.96–103.

Silva, M., Roberts, J.J. and Prado, P.O., 2021. Calculation of the Shading Factors for Solar Modules with MATLAB. *Energies*, 14(15), p.4713.

Skoplaki, E., Boudouvis, A.G. and Palyvos, J.A., 2008. A simple correlation for the operating temperature of photovoltaic modules of arbitrary mounting. *Solar Energy Materials and Solar Cells*, 92(11), pp.1393–1402.

Smith, R.M., Jordan, D.C. and Kurtz, S.R., 2012. *Outdoor PV Module Degradation of Current-Voltage Parameters Preprint OUTDOOR PV MODULE DEGRADATION OF CURRENT-VOLTAGE PARAMETERS*,

Solargis, *Evaluate (Time Series / TMY)* [Online]. Available at: <https://solargis.com/products/evaluate/overview> [Accessed: 6 September 2022].

Soliman, A.M.A., Hassan, H., Ahmed, M. and Ookawara, S., 2020. A 3d model of the effect of using heat spreader on the performance of photovoltaic panel (PV). *Mathematics and Computers in Simulation*, 167, pp.78–91.

Stein, J., Hansen, C. and Reno, M., 2012. *Global horizontal irradiance clear sky models : implementation and analysis.*, Albuquerque, NM, and Livermore, CA (United States).

Thong, L.W., Murugan, S., Ng, P.K. and Chee, S., 2016. Analysis of Photovoltaic Panel Temperature Effects on its Efficiency. March 2016

Varga, N. and Mayer, M.J., 2021. Model-based analysis of shading losses in ground-mounted photovoltaic power plants. *Solar Energy*, 216, pp.428–438.

Yakup, M.A.B.H.M. and Malik, A.Q., 2001. Optimal tilt angle and orientation for solar collector in Brunei Darussalam. *Renewable Energy*, 24(2), pp.223–234.

Yu, C. et al., 2019. Optimal Orientation and Tilt Angle for Maximizing in-Plane Solar Irradiation for PV Applications in Japan. *Sustainability*, 11, p.2016.

APPENDICES

Appendix A: Flowchart for Processing 20-year Solargis Time Series Data

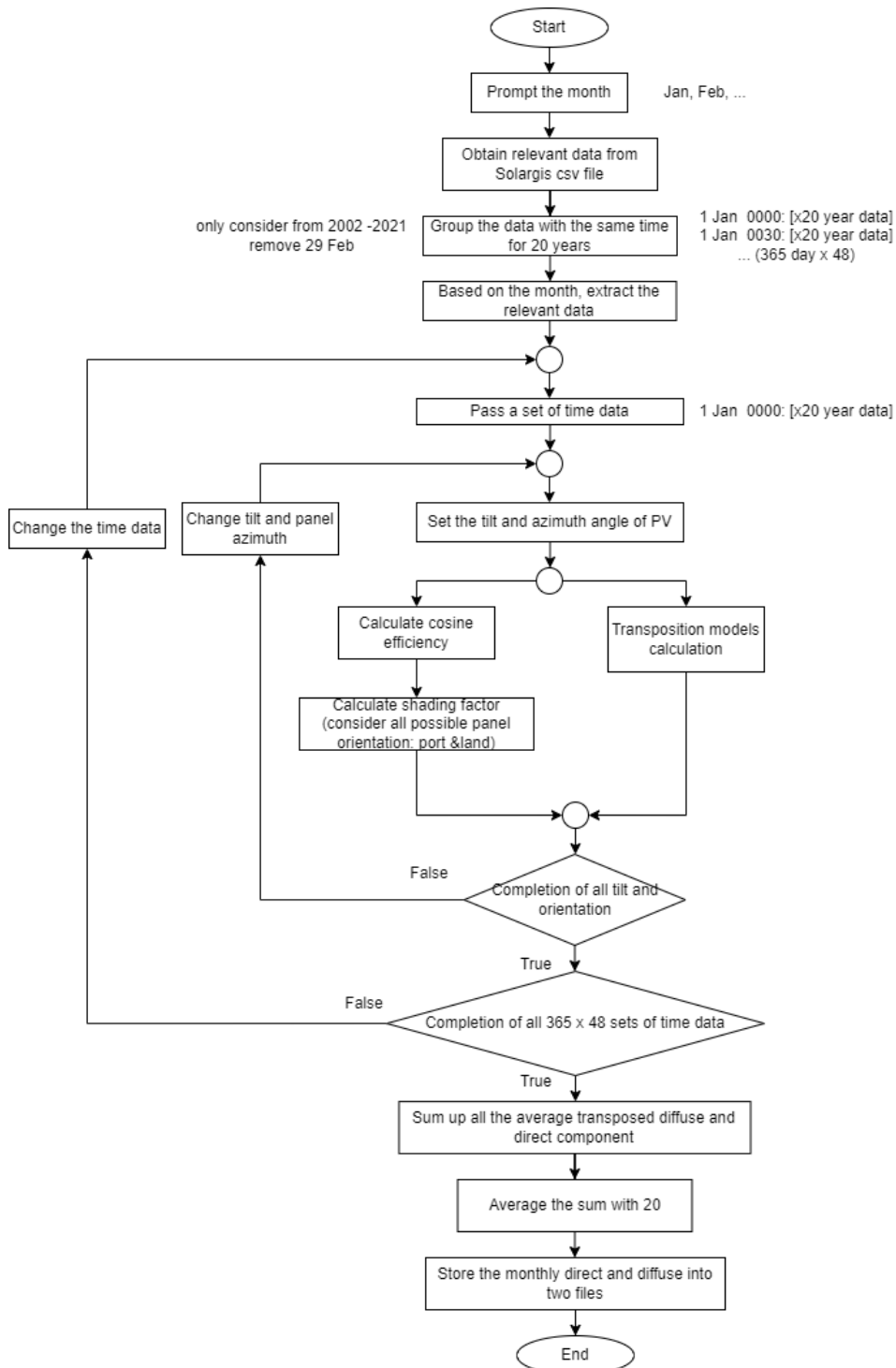


Figure A-1: Flowchart for Computing Average GTI Based on 20-year Solargis Time Series Data